AD-A148 015 RADIATION PARAMETERIZATION PROGRAMS FOR USE IN GENERAL CIRCULATION MODELS(U) UTAH UNIV SALT LAKE CITY DEPT OF METEOROLOGY K N LIOU ET AL. 15 AUG 84 AFGL-TR-84-0217 1/1

UNCLASSIFIED F19628-83-K-0015 F/G 4/2 NL

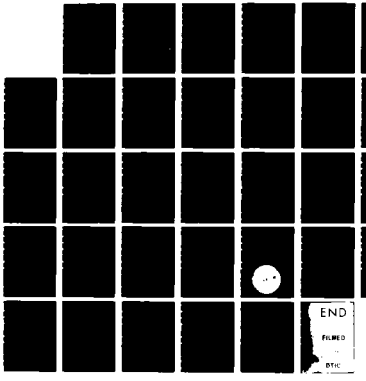

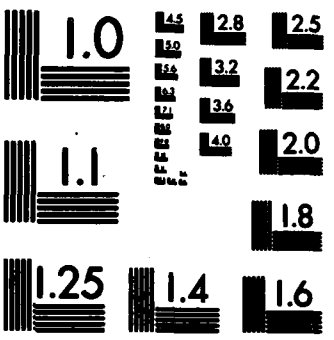

AFGL-TR-84-0217

RADIATION PARAMETERIZATION PROGRAMS FOR USE IN GENERAL CIRCULATION MODELS

Kuo-Nan Liou
Szu-Cheng Ou
Stefan Kinne
George Koenig

Department of Meteorology
University of Utah
Salt Lake City, Utah 84112

Final Report
1 February 1983 - 31 July 1984

15 August 1984

Approved for public release; distribution unlimited

AIR FORCE GEOPHYSICS LABORATORY
AIR FORCE SYSTEMS COMMAND
UNITED STATES AIR FORCE
HANSCOM AFB, MASSACHUSETTS 01731

This report has been reviewed by the ESD Public Affairs Office (PA) and is releasable to the National Technical Information Service (NTIS).

This technical report has been reviewed and is approved for publication.

SAMUEL Y. YEE
Contract Monitor

DONALD A. CHISHOLM, Chief
Atmospheric Prediction Branch

FOR THE COMMANDER

ROBERT A. McCLATCHEY, Director
Atmospheric Sciences Division

Qualified requestors may obtain additional copies from the Defense Technical Information Center. All others should apply to the National Technical Information Service.

If your address has changed, or if you wish to be removed from the mailing list, or if the addressee is no longer employed by your organization, please notify AFGL/DAA, Hanscom AFB, MA 01731. This will assist us in maintaining a current mailing list.

Do not return copies of this report unless contractual obligations or notices on a specific document requires that it be returned.

Unclassified

SECURITY CLASSIFICATION OF THIS PAGE

REPORT DOCUMENTATION PAGE

1a. REPORT SECURITY CLASSIFICATION Unclassified	1b. RESTRICTIVE MARKINGS
2a. SECURITY CLASSIFICATION AUTHORITY	3. DISTRIBUTION/AVAILABILITY OF REPORT Approved for public release; distribution unlimited
2b. DECLASSIFICATION/DOWNGRADING SCHEDULE	
4. PERFORMING ORGANIZATION REPORT NUMBER(S)	5. MONITORING ORGANIZATION REPORT NUMBER(S) AFGL-TR-84-0217
6a. NAME OF PERFORMING ORGANIZATION Department of Meteorology University of Utah 6b. OFFICE SYMBOL (If applicable)	7a. NAME OF MONITORING ORGANIZATION Air Force Geophysics Laboratory
6c. ADDRESS (City, State and ZIP Code) Salt Lake City, Utah 84112	7b. ADDRESS (City, State and ZIP Code) Hanscom AFB Massachusetts 01731 Monitor/Samuel Yee/LYP
8a. NAME OF FUNDING/SPONSORING ORGANIZATION 8b. OFFICE SYMBOL (If applicable)	9. PROCUREMENT INSTRUMENT IDENTIFICATION NUMBER F19628-83-K-0015
8c. ADDRESS (City, State and ZIP Code)	10. SOURCE OF FUNDING NOS.

PROGRAM ELEMENT NO.	PROJECT NO.	TASK NO.	WORK UNIT NO.
61102 F	2310	G7	AF

11. TITLE (Include Security Classification) Radiation Parameterization Programs for Use in General Circulation Models

12. PERSONAL AUTHOR(S)
Kuo-Nan Liou, Szu-Cheng Ou, Stefan Kinne and George Koenig

13a. TYPE OF REPORT	13b. TIME COVERED	14. DATE OF REPORT (Yr., Mo., Day)	15. PAGE COUNT
Final Report	FROM 2/1/83 TO 7/31/84	1984 August 15	59

16. SUPPLEMENTARY NOTATION
NA

17. COSATI CODES		
FIELD	GROUP	SUB. GR.

18. SUBJECT TERMS (Continue on reverse if necessary and identify by block number)
Infrared radiation, Solar radiation, Radiative transfer, Parameterization, Cloud, University of Utah (UU), General Circulation Model, AFGL six-layer baseline model

19. ABSTRACT (Continue on reverse if necessary and identify by block number)

→ Parameterization programs involving infrared and solar radiation transfer in clear and cloudy atmospheres containing high and low cloud systems are described in this report. We document in detail the physical concepts and basic parameterization equations used for the computation of infrared and solar fluxes in clear and cloudy atmospheres along with the verification of various parameterization programs. In addition, we illustrate some preliminary results of the global distributions of the cloud and radiation budget generated from the AFGL model with the incorporation of the present radiation-cloud parameterization programs. Finally, we provide a detailed description of the radiation parameterization computer programs including the programming interface with the AFGL six-layer general circulation model.

20. DISTRIBUTION/AVAILABILITY OF ABSTRACT	21. ABSTRACT SECURITY CLASSIFICATION
UNCLASSIFIED/UNLIMITED ☐ SAME AS RPT. ☒ DTIC USERS ☐	Unclassified

22a. NAME OF RESPONSIBLE INDIVIDUAL	22b. TELEPHONE NUMBER (Include Area Code)	22c. OFFICE SYMBOL
Samuel Yee	(617) 861-2128	AFGL/LYP

DD FORM 1473, 83 APR EDITION OF 1 JAN 73 IS OBSOLETE.

Unclassified

SECURITY CLASSIFICATION OF THIS PAGE

TABLE OF CONTENTS

Publications

The research work contained in the following publications has been supported in part by the Air Force Geophysics Laboratory under contracts F19628-81-K-0042 and F19628-83-K-0015.

1. Liou, K.N. and S.C. Ou, 1981: Parameterization of infrared radiative transfer in cloudy atmospheres. J. Atmos. Sci., 38, 2707-2716.

2. Hutchison, K. and K.N. Liou, 1983: Parameterization of broadband solar radiation transfer in clear and cloudy atmospheres. Scientific Report, Air Force Geophysics Laboratory, AFGL-TR-82-0364, ADA123396.

3. Liou, K.N. and S.C. Ou, 1983: Theory of equilibrium temperatures in radiative-turbulent atmospheres. J. Atmos. Sci., 40, 214-229.

4. Ou, S.C. and K.N. Liou, 1983: Parameterization of carbon dioxide 15 μm absorption and emission. J. Geophys. Res., 88, 5203-5207.

5. Liou, K.N. and Q. Zheng, 1984: A numerical experiment on the interactions of radiation, clouds and dynamic processes in a general circulation model. J. Atmos. Sci., 41, 1513-1535.

Acknowledgements

David Doehing assisted in the preparation of Figs. 11, 12, 13 and 14. Sharon Bennett typed and edited the final report. Major Keith Hutchison contributed the solar radiation parameterization program during his stay at the University of Utah.

Section 1

INTRODUCTION

Under the sponsorship of the Meteorology Division of the Air Force Geophysics Laboratory (AFGL) we have undertaken the development of a parameterization program involving the transfer of thermal infrared and solar radiation in clear and cloudy atmospheres. The prime objective of this program is to construct a unified and coherent radiation package, including cloud contributions, which is computationally economic yet numerically reliable and stable, for the incorportation into a global dynamic model. Thus, our radiation and cloud programs are closely in line with the overall AFGL effort in developing a global model for short and medium range weather and cloud forecast research.

In this report, we describe the infrared and solar radiation parameterization programs developed at the University of Utah over the period supported by AFGL. In Sections 2 and 3, we present detailed descriptions of the physical concepts and basic parameterization equations developed for the computation of infrared and solar fluxes in clear and cloudy atmospheres. Verifications of the IR and solar radiation parameterization programs also are given in these sections. In addition, we present in Section 4 some preliminary results of the global distributions of clouds and radiation budgets generated from the AFGL model utilizing the atmospheric data corresponding to 15 January 1978. Finally, detailed documentation of the radiation parameterization programs including the

programming interface with the AFGL six-layer general circulation model is given in the Appendix.

Section 2

INFRARED RADIATION PROGRAM

2.1 Clear Atmosphere

Following the analysis presented by Liou (1980) utilizing the broadband emissivity concept, the upward and downward infrared fluxes at a given level in a clear atmosphere may be written in the forms

$$F^{\uparrow}(z) = \sigma T_*^4 \left[1 - \varepsilon^f(z,T_*)\right] + \int_0^z \sigma T^4(z') \, K(z-z') \, dz' \tag{2.1}$$

$$F^{\downarrow}(z) = \int_{z_\infty}^{z} \sigma T^4(z') \, K(z'-z) \, dz' \tag{2.2}$$

where the broadband flux emissivity and the atmospheric kernel function are defined by

$$\varepsilon^f(z,T_*) = \sum_{i=1}^{6} \varepsilon_i^f \left[\tilde{u}_i(z), T_*\right] \tag{2.3}$$

$$K(z-z') = -\frac{d}{dz'} \varepsilon^f \left[z-z', T(z')\right]$$

$$= -\frac{d}{dz'} \sum_{i=1}^{6} \varepsilon_i^f \left[\tilde{u}_i(z) - \tilde{u}_i(z'), T(z')\right] \tag{2.4}$$

In these equations, T_* denotes the surface temperature, $u_1 = u_2 = u_3 = u_w$, the water vapor path length, $u_4 = u_c$, the carbon dioxide path length, and $u_5 = u_o$, the ozone path length. ε_i^f (i = 1-5) are the individual broadband emissivities for the H_2O rotational band, H_2O vibrational-

rotational band, H_2O continuum, CO_2 and O_3 bands, respectively. The broadband emissivity corresponding to the H_2O-CO_2 overlap correction is given by $\varepsilon_6^f(\tilde{u}_6) = -\varepsilon_1^f(\tilde{u}_w)\ \varepsilon_4^f(\tilde{u}_c)$. In Eqs. (2.3) and (2.4), $\tilde{u}_i$ denotes the pressure and temperature corrected path length defined below for each band. The individual broadband emissivities are defined by

$$\varepsilon_i^f(\tilde{u}_i,T) = \sum_n \pi B_{\nu_n}(T)\ [1 - T_{\nu_n}^f(\tilde{u}_i)]\ \Delta\nu_n/\sigma\ T^4\ , \qquad (2.5)$$

where n denotes the number of spectral intervals $\Delta\nu_n$, πB_{ν_n} the spectral Planck flux, and the spectral slab (or diffuse) transmittance $T_\nu^f(\tilde{u}) \approx T_\nu$ (1.66 $\tilde{u}$). The spectral transmittance T_ν is obtained either from theoretical band models or from detailed absorption line data involving the line position, line strength and half width.

2.1.1 Water Vapor

For the three water vapor absorption bands we use the broadband emissivity curves in terms of polynomial functions presented by Liou and Ou (1983). In their approach, the broadband emissivities for water vapor pure rotational and vibrational-rotational bands are derived from the random band parameters assuming Lorentz line shapes obtained by Rodgers and Walshaw (1966) in which an empirical temperature correctior for the rotational band was also given. For the water vapor continuum absorption in the window regions, the empirical formula developed by Roberts et al. (1976) was used. The polynomial functions have the form

$$\ell n\ \varepsilon_i^f(\tilde{u}_i,T) = \sum_{n=0}^{3} a_{n,i}\ \bar{u}_i^n,\quad \bar{u}_i = (2\ \log_{10}\tilde{u}_i - \bar{a})\ /\ \bar{b} \qquad (2.6)$$

where

$$\bar{a} = \log_{10} (\tilde{u}_{i,max}\, \tilde{u}_{i,min}), \quad \bar{b} = \log_{10} (\tilde{u}_{i,max} / \tilde{u}_{i,min})$$

with $\tilde{u}_{i,max}$ (= 10^{10} g cm^{-2}) and $\tilde{u}_{i,min}$ (= 10^{-7} g cm^{-2}) representing the maximum and minimum path lengths used in the numerical fitting. The pressure and temperature corrected path lengths are (Liou and Ou, 1981)

$$\tilde{u}_1 = \int_0^z \frac{P(z')}{P_0} \exp \left\{ A' [T(z') - T_a] + B' [T(z') - T_a]^2 \right\} \rho_w(z')\, dz', \tag{2.7}$$

$$\tilde{u}_2 = \int_0^z \frac{P(z')}{P_0} \rho_w(z')\, dz' , \tag{2.8}$$

$$\tilde{u}_3 = \int_0^z \frac{P_w(z')}{P_{0w}} \exp \left\{ - \frac{1800}{T_b T(z')} [T(z') - T_b] \right\} \rho_w(z')\, dz' , \tag{2.9}$$

where $A' = 10.6278 \times 10^3$ K^{-1}, $B' = -44.6132 \times 10^{-6}$ K^{-2}, $T_a = 260°$ K, $T_b = 296°$ K, $P_0 = 1013$ mb, P_w and P_{0w} are vapor pressure at temperatures T and T_b, respectively and ρ_w is the water vapor density. Table 1 lists the coefficients of the broadband emissivity equation $a_{n,i}$ for three water vapor bands (i = 1,2,3). As illustrated in the paper by Liou and Ou (1983), the clear column cooling rates due to water vapor absorption and emission in the troposphere agree well with results from line-by-line calculations. Pertinent results will be duplicated in this report for documentation purposes.

2.1.2 Carbon Dioxide

The broadband emissivity for carbon dioxide is computed using the parameterization scheme recently developed by Ou and Liou (1983). In that paper the CO_2 broadband emissivity, which is a function of the pressure and temperature corrected path length $\tilde{u}_c$ and the atmospheric temperature, is derived from the line-by-line transmittance data presented by Fels and Schwarzkopf (1981). It is fitted by the following equations:

Table 1. Coefficients of Broadband Emissivity Values for Water Vapor and Ozone Bands.

	i	$a_{0,i}$	$a_{1,i}$	$a_{2,i}$	$a_{3,i}$
T = 203° K	1	-.16378+001	.31523+001	-.28231+001	.10998+001
	2	-.98069+001	.91563+001	-.54110+000	-.27859+000
	3	-.58349+001	.54245+001	-.34050+001	.85649-002
	5	-.67785+001	.42930+001	-.95681+000	-.55536+000
T = 233° K	1	-.18865+001	.32475+001	-.27705+001	.10903+001
	2	-.95159+001	.91534+001	-.52756+000	-.26671+000
	3	-.50133+001	.53627+001	-.34506+001	.10991-001
	5	-.63805+001	.42918+001	-.95672+000	-.55860+000
T = 263° K	1	-.21226+001	.33251+001	-.27277+001	.10832+001
	2	-.93430+001	.91512+001	-.51723+000	-.25749+000
	3	-.44264+001	.53278+001	-.34806+001	.79503-002
	5	-.61317+001	.42910+001	-.95628+000	-.56004+000
T = 293° K	1	-.23454+001	.33888+001	-.26927+001	.10777+001
	2	-.92462+001	.91495+001	-.50918+000	-.25017+000
	3	-.39991+001	.53068+001	-.35005+001	.42209-002
	5	-.59797+001	.42904+001	-.95611+000	-.56109+000

$$\ln \varepsilon_4^f(\tilde{u}_c,T) = \sum_{n=0}^{3} a_n \tilde{u}'^n, \quad \text{for } \tilde{u} \geq 10^{-4} \text{ g cm}^{-2} \tag{2.10a}$$

$$\ln \varepsilon_4^f(\tilde{u}_c,T) = b_0 + b_1 \tilde{u}', \quad \text{for } \tilde{u} < 10^{-4} \text{ g cm}^{-2} \tag{2.10b}$$

where

$$\tilde{u}' = (2 \log \tilde{u} + 7.69897) / 6.30103$$

and $a_0 = -4.00893 + f(T)$, $a_1 = 4.39628$, $a_2 = -3.07709$, $a_3 = 0.94529$, $b_0 = -4.00036 + f(T)$, and $b_1 = 5.13453$. $f(T) = \ln \{h(T)\, g(T)/[h(T_0)\, g(T_0)]\}$, where $h(T) = 1 + A\,\Delta T(1 - B\Delta T)$, $g(T) = \int_{\nu_1}^{\nu_2} \pi B_\nu(T)\, d\nu/\sigma T^4$, $A = 1.833 \times 10^{-4}$, $B = 1.364 \times 10^{-2}$, $\Delta T = T - 250$, $\nu_1 = 500$ cm^{-1} and $\nu_2 = 850$ cm^{-1}. The pressure and temperature corrected path lengths have the form

$$\tilde{u}_4 = 2c \Big/ \left\{ [1 + 4(c^2 / u^2 + c / \bar{u})]^{1/2} - 1 \right\} \tag{2.11}$$

where the constant $c = 3.7551 \times 10^{-4}$ g cm^{-2} and

$$\bar{u} = \int_0^z \frac{P(z')}{P_0} \left[\frac{T_0}{T(z')}\right]^{1/2} \rho_c(z')\, dz' \tag{2.12}$$

with ρ_c the carbon dioxide density and $T_0 = 273°$ K. CO_2 cooling rates calculated from the broadband emissivity parameterization approach show a maximum difference of 0.5° C/day when they are compared with those computed from exact line-by-line integrations utilizing standard and polar atmospheric temperature profiles.

2.1.3 Ozone

As for ozone, random model parameters for the 9.6 μm band derived by Goldman and Kyle (1968) are utilized to derive the O_3 broadband emissivity which is also fitted in terms of the polynomial function [Eq. (2.6)]. However, the maximum and minimum path lengths used in the fitting are 10^{-3} and 10^{-7} g cm^{-2}, respectively. Because of the uncertainty of applying pressure and temperature corrections to the path

length in the cooling rate calculation due to ozone, no adjustment has been made. Table 1 also lists the coefficients of the broadband emissivity equation for the ozone band. The calculation of ozone cooling rates is certainly an area requiring further improvement especially when the stratosphere is to be incorporated in the dynamic model.

2.2 Cloudy Atmosphere

We shall consider a two-layered cloud system having a semi-transparent and non-black high cloud aloft coupled with a black cloud below. Let the infrared broadband emissivity, transmissivity and reflectivity for the high cloud be denoted as ε^c, t^c and r^c, respectively. For black clouds, we let $\varepsilon^c = 1$ and $t^c = r^c = 0$ for simplicity of treating the infrared flux exchange. In a manner similar to, but not exactly the same as, the parameterization equations given by Liou and Ou (1981), we may express the upward and downward fluxes at a given level (Fig. 1) above the high cloud, between high and progressively lower clouds, and below the lower cloud.

For heights above the high cloud top, we have

$$F^{\downarrow}(z) = \int_{z_\infty}^{z} \sigma T^4(z')\, K(z'-z)\, dz' \,, \tag{2.13}$$

$$\begin{aligned} F^{\uparrow}(z) = {} & r^c \int_{z_\infty}^{z_{t1}} \sigma T^4(z')\, K(z'+z-2z_{t1})\, dz' \\ & + t^c \Big\{ \sigma T_{t2}^4 \left[1 - \varepsilon^f (z_{b1}-z_{t2}+z-z_{t1}, T_{t2})\right] + \int_{z_{t2}}^{z_{b1}} \sigma T^4(z')\, K(z-z_{t1}+z_{b1}-z')\, dz' \\ & + \varepsilon_{t1}^c\, \sigma T_{t1}^4 \left[1 - \varepsilon^f (z-z_{t1}, T_{t1})\right] + \int_{z_{t1}}^{z} \sigma T^4(z')\, K(z-z')\, dz' \,, \\ & \qquad z_{t1} < z < z_\infty \end{aligned} \tag{2.14}$$

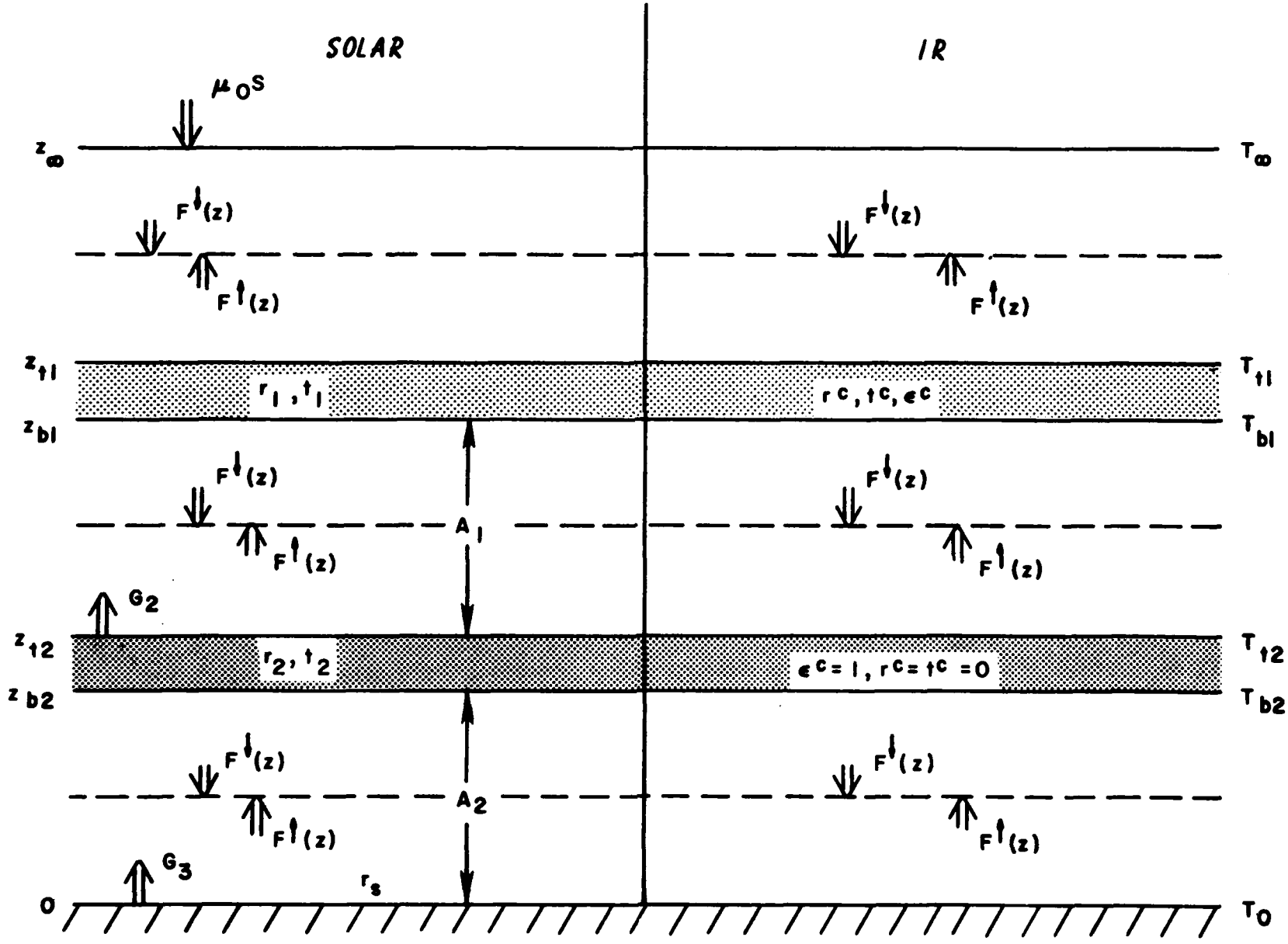

Fig. 1 Geometrical configuration of solar and IR flux transfer in an atmosphere containing two cloud layers.

Below the high cloud base and above the low cloud top, we obtain

$$F^{\uparrow}(z) = \sigma T_{t2}^4 \left[1 - \varepsilon^f (z-z_{t2}, T_{t2})\right] + \int_{z_{t2}}^{z} \sigma T^4(z')\, K(z-z')\, dz' \,, \quad (2.15)$$

$$F^{\downarrow}(z) = r^c \left\{ \sigma T_{t2}^4 \left[1 - \varepsilon^f (2z_{b1}-z_{t2}-z, T_{t2})\right] + \int_{z_{t2}}^{z} \sigma T^4(z')\, K(2z_{b1}-z-z')\, dz' \right\}$$

$$+ t^c \int_{z_\infty}^{z_{t1}} \sigma T^4(z')\, K(z'-z_{t1}+z_{b1}-z)\, dz'$$

$$+ \left\{ \varepsilon_{b1}^c\, \sigma T_{b1}^4 \left[1 - \varepsilon^f (z_{b1}-z, T_{b1})\right] + \int_{z_{t2}}^{z} \sigma T^4(z')\, K(z'-z)\, dz' \right\}, \quad (2.16)$$

$$z_{t2} < z < z_{b1}$$

Below the low cloud base, the fluxes are related to two black surfaces and are simply given by

$$F^{\uparrow}(z) = \sigma T_{\star}^4 \left[1 - \varepsilon^f (z, T_{\star})\right] + \int_{0}^{z} \sigma T^4(z')\, K(z-z')\, dz' \quad (2.17)$$

$$F^{\downarrow}(z) = \sigma T_{b2}^4 \left[1 - \varepsilon^f (z_{b2}-z, T_{b2})\right] + \int_{z_{b2}}^{z} \sigma T^4(z')\, K(z-z')\, dz' \quad (2.18)$$

$$0 < z < z_{b2}$$

When there is only one cloud generated in the model, we set $z_{b2} = z_{t2} = z_{b1}$ and $T_{b2} = T_{t2} = T_{b1}$. Thus, only Eqs. (2.13) - (2.16) are required in the computation. Note that except for single high clouds, all other cloud types are considered to be black reflectively.

The broadband infrared emissivity, reflectivity and transmissivity for cirrus are functions of the vertical ice content following the

parameterization equation developed by Liou and Wittman (1979) in the form

$$R(W) = \sum_{i=0}^{5} c_i W^i \tag{2.19}$$

where R(W) denotes the flux reflectivity, transmissivity or emissivity of the cirrus cloud, c_i the predictor coefficients listed in Table 2, and W the vertical ice content in units of 10^2 g m^{-2}.

For partly cloudy conditions, the infrared cooling rate at each model layer is obtained by weighting linearly the percentage of the fractional cloud cover c and the percentage of the clear portion in the form

$$\left(\frac{\partial T}{\partial t}\right)^{pc} = c \left(\frac{\partial T}{\partial t}\right)^{c} + (1 - c) \left(\frac{\partial T}{\partial t}\right)^{nc} \tag{2.20}$$

Table 2. Approximating predictor coefficients c_i for a cirrus cloud in the infrared region.

i	Reflectivity	Transmissivity	Emissivity
0	0.30619E - 01	0.73597E + 00	0.28568E + 00
1	0.81134E + 00	-0.38162E + 01	0.35222E + 01
2	-0.18995E + 01	0.83288E + 01	-0.76275E + 01
3	0.24900E + 01	-0.91066E + 01	0.83096E + 01
4	-0.15805E + 01	0.48765E + 01	-0.44405E + 01
5	0.37581E + 00	-0.10141E + 01	0.92209E + 00

This equation is also applicable to solar heating rate calculations in partly cloudy conditions.

The radiative heating rate at level z is related to the divergence of net fluxes and is given by

$$\frac{\partial T}{\partial t} = \mp \frac{1}{\rho C_p \Delta z} \Delta \left[F^{\uparrow}(z) - F^{\downarrow}(z)\right] , \qquad (2.21)$$

where ρ is the air density, C_p the specific heat at constant pressure and Δz the model layer thickness. The negative and positive signs are applicable to infared and solar radiation, respectively.

2.3 Verification of IR Parameterization Program

Utilizing the broadband emissivity approach denoted in Sections 2.1 and 2.2, we have carried out a number of numerical comparisons and verifications with more detailed band-by-band and/or line-by-line calculations (Liou and Ou, 1981; Ou and Liou, 1983). Below, we present some highlights of these comparisons.

In Fig. 2, we first illustrate comparisons of infrared cooling results using band-by-band and broadband approaches for water vapor and ozone components. For the water vapor component, the broadband approach reproduces fairly accurately the cooling rate below about 20 km when it is compared with the band-by-band approach with differences within about 0.3°C day^{-1}. The present results show reasonable agreement with those obtained from a more exact line-by-line calculation. Note that cooling results from the line-by-line method are available only for heights between 3 and 25 km. At above 35 km the broadband value differs from the band-by-band result by as much as 1°C day^{-1}.

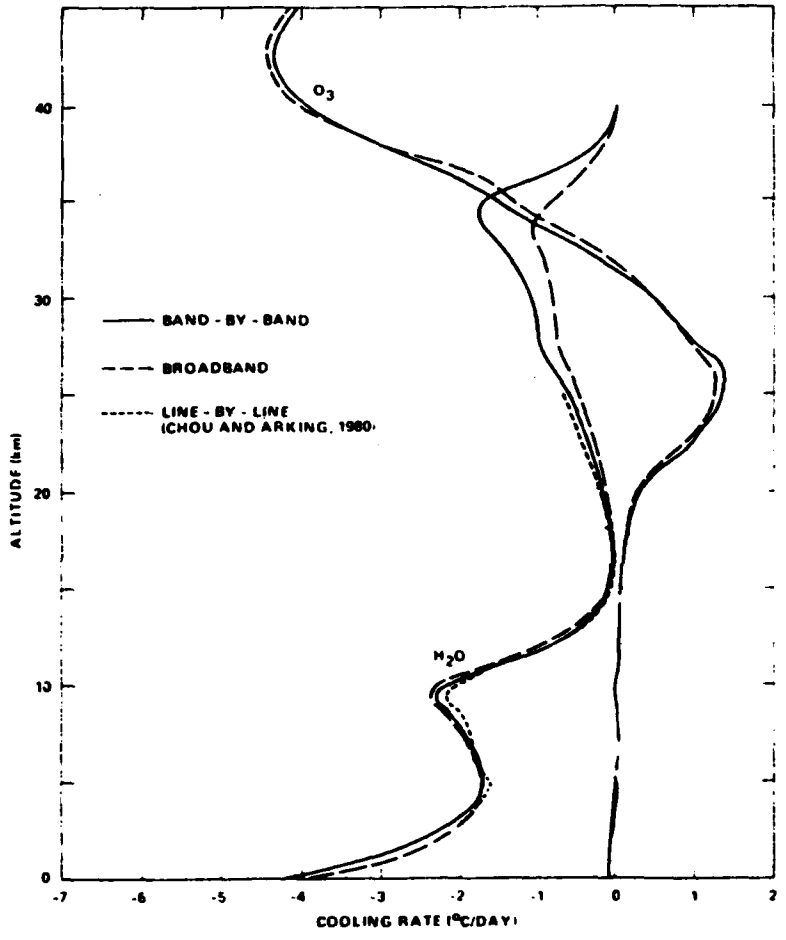

Fig. 2a. Comparison of cooling rate profiles for water vapor, carbon dioxide, and ozone computed from the band-by-band and broadband emissivity methods. Also shown is the water vapor cooling rate profile calculated from a line-by-line program (Chou, personal communication). A tropical atmospheric profile is used in these calculations.

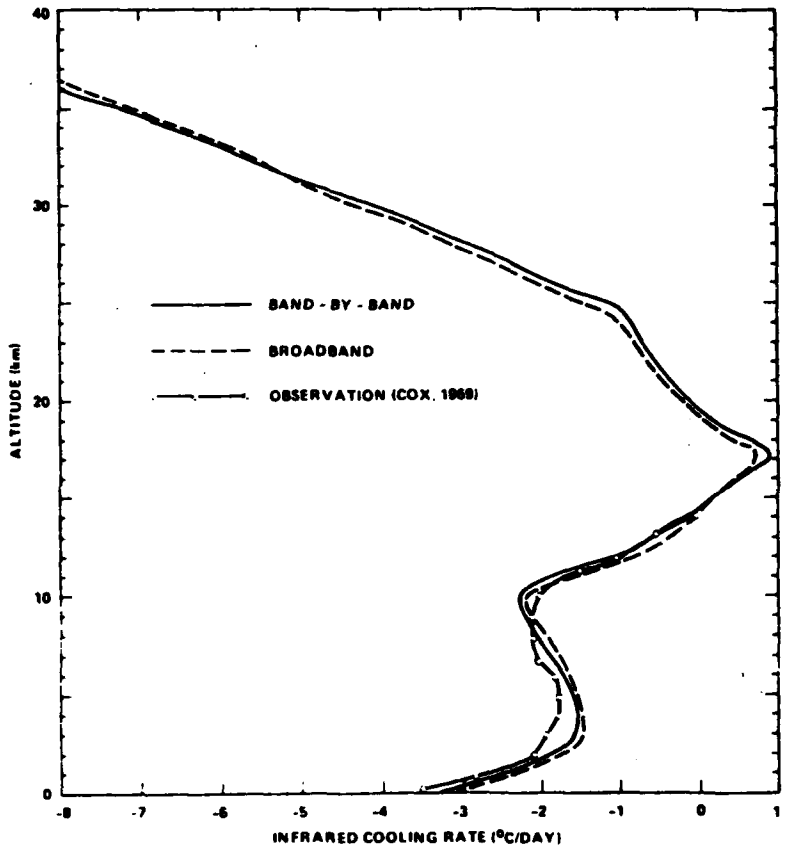

Fig. 2b. Comparison of total cooling rate profiles for a clear tropical atmosphere computed from the band-by-band and broadband emissivity methods. An observed cooling rate profile in the tropics reported by Cox (1969) also is depicted.

This larger deviation is in part due to the cut-off of water vapor concentration at a height of 45 km where cooling drops to zero. We note, however, that cooling due to water vapor at about 20 km is relatively insignificant compared with that of carbon dioxide and ozone. As for the ozone component, agreement between results from the broadband and band-by-band methods are excellent with differences held to within 0.2°C day^{-1}. Note that ozone shows heating on the order of 1°C day^{-1} at ~25 km, corresponding to the ozone maximum.

In our previous program (Liou and Ou, 1981), we used the random band parameters calculated by Rodgers and Walshaw (1966) for H_2O and CO_2 to derive the broadband emissivities and overlap contributions. Since they only gave one CO_2 band value, the CO_2 broadband emissivity computed from one band value is generally less accurate, especially for atmospheres above about 35 km. For this reason, we have improved the parameterization of the CO_2 broadband emissivity based on line-by-line data given by Fels and Schwazkopf (1981). In Fig. 3, infrared cooling rates due to the 15 μm CO_2 band are shown utilizing standard and polar temperature profiles (Ou and Liou, 1983). Also included in the figure are a number of published results. From these comparisons, it is noted that the present results differ from those of Fels and Schwarzkopf (1981) who employed a line-by-line technique by no more than 5%. It should be noted that the new CO_2 emissivity parameterization will affect flux and cooling rate calculations only above about 35 km.

Moreover, we present total cooling rates due to H_2O, CO_2 and O_3 computed from the present parameterization program and compare them

with those calculated from a more elaborate band-by-band method. This comparison is shown in Fig. 2b. Also depicted in the figure is the observed cooling profile in the tropics presented by Cox (1969). Although the atmospheric water vapor and temperature profiles corresponding to the observed cooling rate may not be exactly the same as those for the tropical atmosphere used in theoretical calculations, the comparison does serve as a general check on the reliability of the theoretical result. Results from the broadband parameterization method are less than the band-by-band values by ~0.2-0.5°C day^{-1}. Moreover, we see that the theoretical cooling rates are in general agreement with the observed values in the troposphere. In the stratosphere the total cooling profile derived from the broadband approach shows a close comparison with that from the band-by-band method, with differences generally less than about 0.2°C day^{-1}. In a clear tropical atmosphere the infrared cooling profile shows a number of maxima and minima, in addition to the strong cooling in the upper atmosphere due to carbon dioxide and ozone. The minimum at ~17 km is known as a basic result of the temperature inversion at the tropopause. The maximum at ~10 km and the minimum at ~3 km are associated with the nonlinear interaction of temperature and emissivity slopes. The latter slope is further associated with the water vapor concentration profile.

In addition, in Fig. 4 is shown an infrared cooling rate profile generated from the present broadband emissivity method for the standard atmospheric condition. Also illustrated in the figure for comparison purposes are results presented by Manabe and Strickler (1964) and by Dickinson (1973) for atmospheres above 30 km. Cooling rates derived

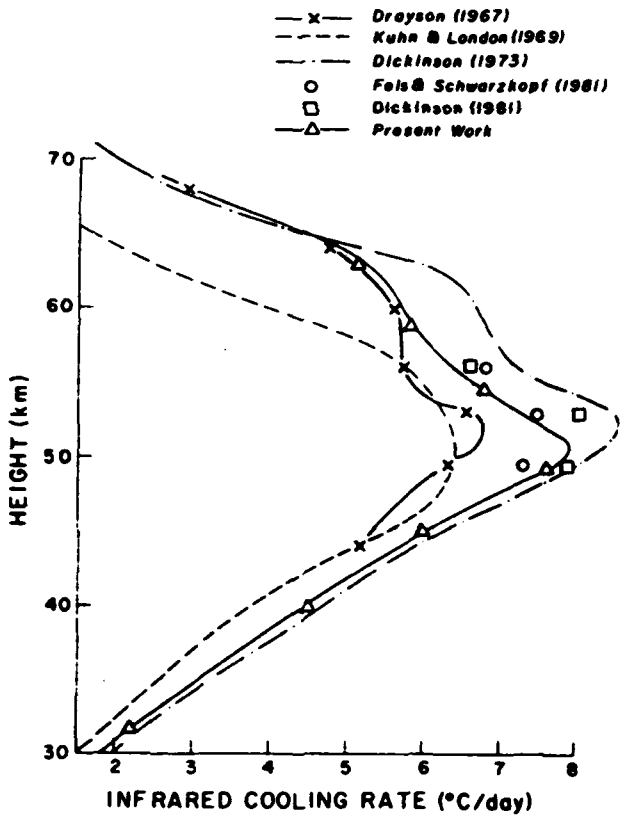

Fig. 3a. Comparison of the infrared cooling rates due to the 15 μm CO_2 band obtained from the present parameterization scheme and those from publised results for a standard atmosphere.

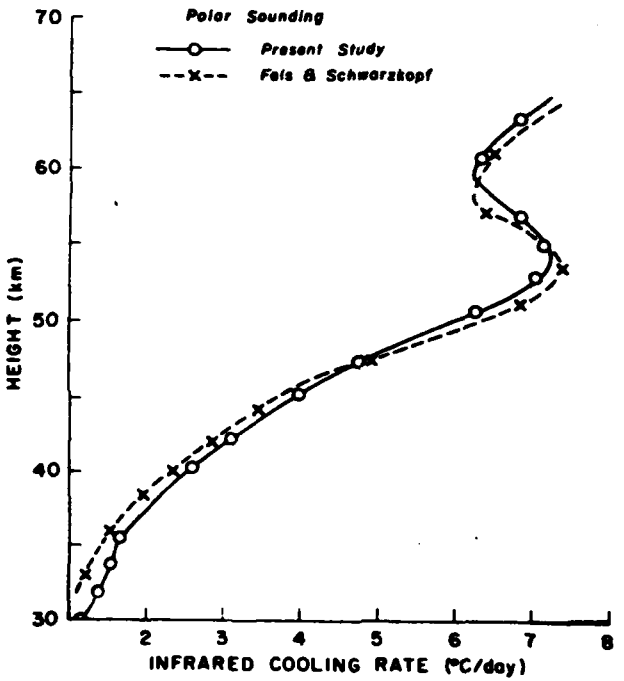

Fig. 3b. Comparison of the infrared cooling rates due to the 15 μm CO_2 band obtained from the present parameterization scheme and that from the method of Fels and Schwarzkopf (1981) for a polar temperature profile depicted in Figure 1 of their paper.

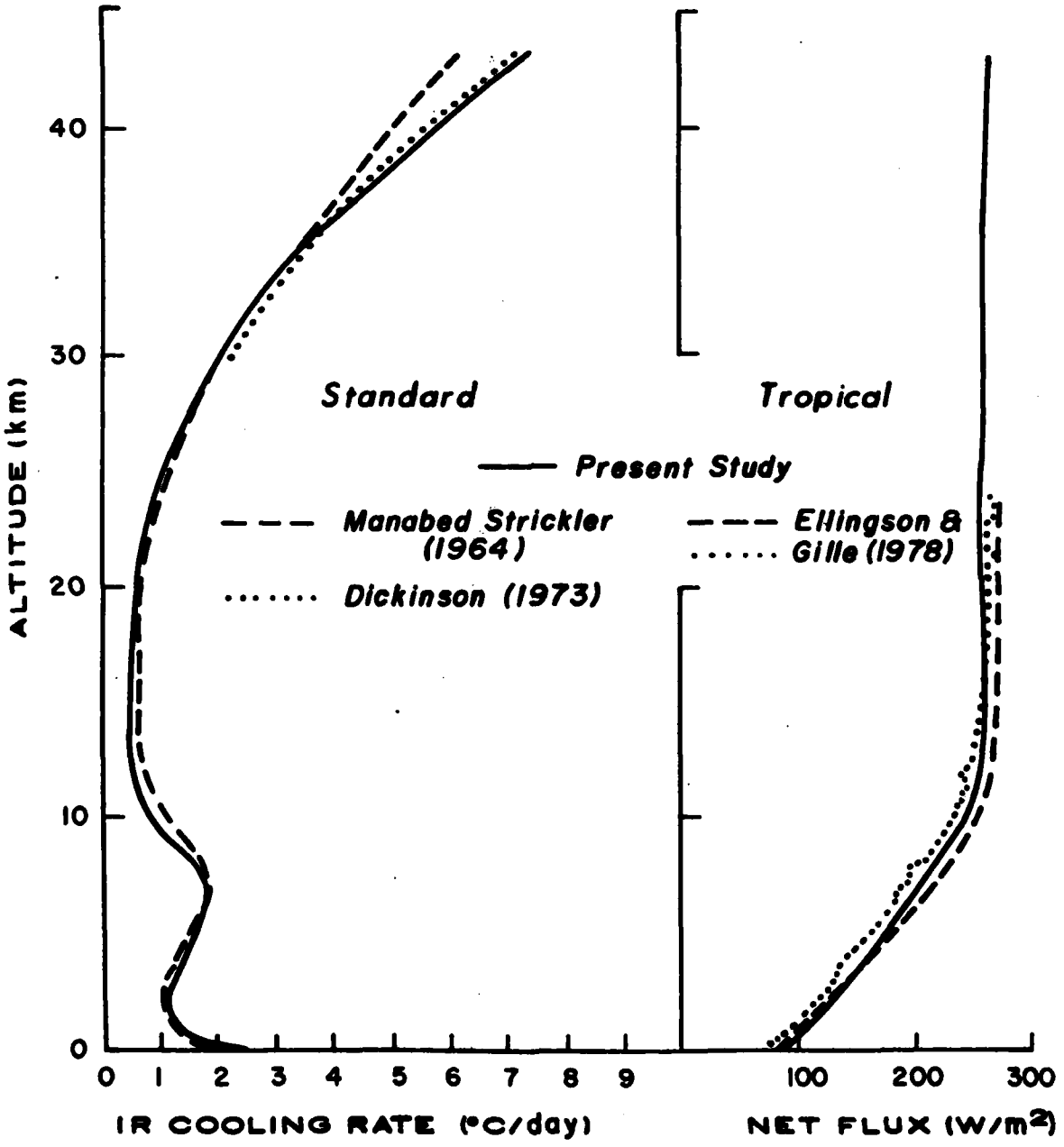

Fig. 4 Comparisons of the infrared cooling rates and net fluxes computed from the present study with other published results. Dots in the net flux diagram denote radiometersonde observations reported in Ellingson and Gille (1978).

from the present study compare well with Dickinson's results. We show larger cooling rates than those presented by Manabe and Strickler below about 6 km. Basically, this is due to the incorpcration of water vapor continuum absorption in the present study. The general differences between the present study and that of Manabe and Strickler may be attributed to the vertical resolution and emissivity method employed in the calculation. The right-hand graph in this figure illustrates the infrared net flux profiles for a tropical atmosphere computed from the present study. Also depicted in the diagram for comparison purposes are results presented by Ellingson and Gille (1978). The dashed line and dots are net flux profiles based on their model calculation and radiometersonde observations, respectively, reproduced from Fig. 14 of their paper. There is a close agreement of the infared net fluxes between model computations within about 5 W m^{-2} below about 10 km. Between about 10-24 km, differences increase to within about 15 W m^{-2}. The present results computed in the height coordinate appear to compare more closely with observed net flux data. Note that the computations of cooling rates and net fluxes utilize two different atmospheric profiles so as to have adequate comparisons with other published results.

Finally, we show in Fig. 5 infrared cooling rate profiles in cirrus cloudy atmospheres employing the technique described in Section 2.2 and compare these with results derived from a band-by-band model (Liou and Ou, 1981). Tropical atmospheres containing a 0.1 and a 3 km non-black cirrus with a base height of 8 km were used in the calculations. For the 0.1 km cirrus case shown in Fig. 5a, except near the cloud top and bottom, the parameterization approach gives reasonably accurate

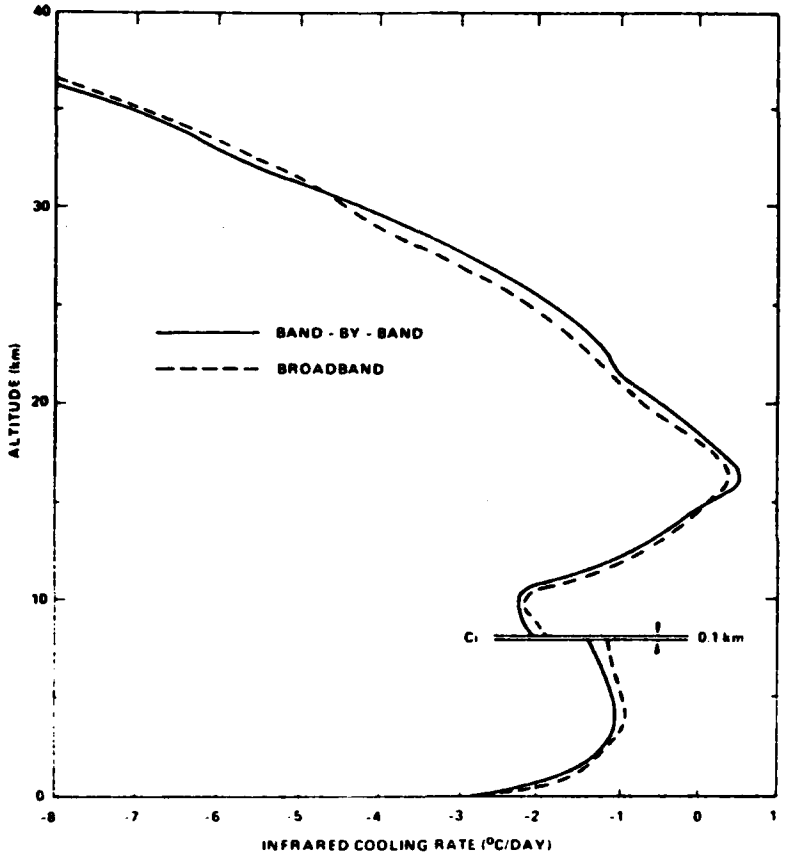

Fig. 5a Comparison of total cooling rate profiles for a tropical atmosphere containing a 0.1 km cirrus cloud computed from band-by-band and broadband methods.

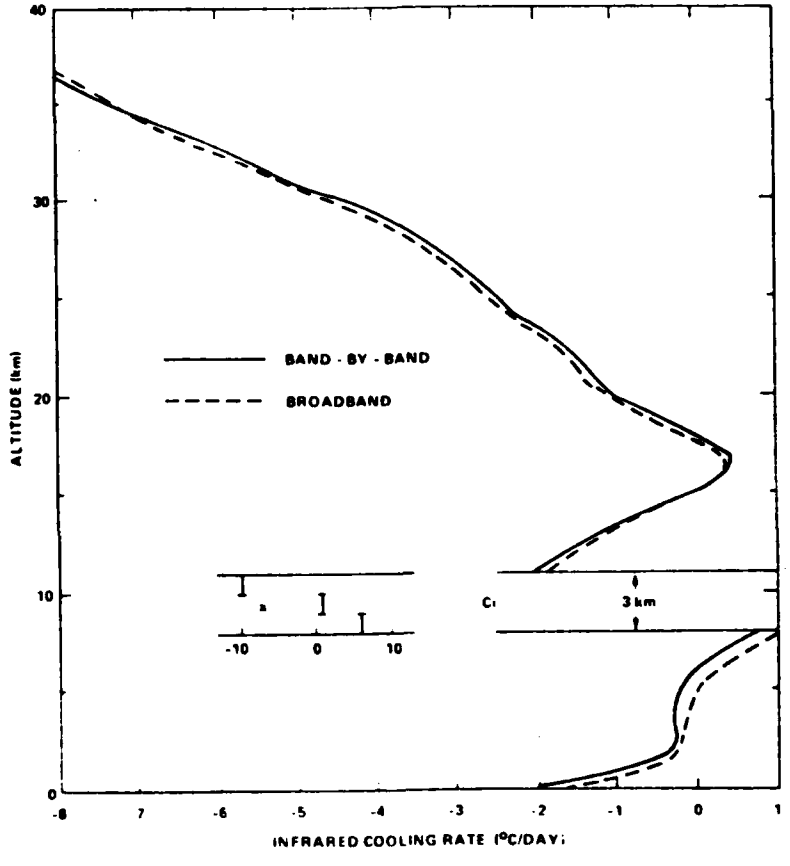

Fig. 5b. Comparison of total cooling rate profiles for a tropical atmosphere containing a 3 km cirrus cloud computed from band-by-band and broadband methods. Cooling rates within the cloud also are depicted.

cooling values as compared to results computed from a more detailed band-by-band method. The larger cooling deviation is caused by the inability of the broadband calculation to obtain very accurate net fluxes near the thin cloud region. The most significant and pronounced effect of non-black cloud is the suppression of cooling below the cloud. The cooling rate is reduced by as much as 1°C day^{-1} everywhere below a 0.1 km cloud. The cooling profile involving a 3 km cirrus cloud is shown in Fig. 5b where we also find a consistent accuracy of the broadband emissivity approach relative to the band-by-band method. The vertical ice content in this case amounts to 156.8 g m^{-2} which generates infrared broadband reflectivity and emissivity of 0.2401 and 0.9876, respectively, with a zero transmissivity. As far as the conventional definition of the emissivity is concerned, the 3 km cirrus almost approaches a blackbody. However, we see a significant component of reflected flux from an almost black cloud due to the scattering of infrared radiation by cloud particles. The contribution of reflection and cloud bottom emission produces heating instead of cooling for atmospheres between the cloud bottom and about 5 km height. The reflection component attributes to ~20% of heating in this case. Moreover, the surface infrared cooling is also much reduced, by ~2°C day^{-1}. On the other hand, atmospheric cooling is enhanced as much as 1-2°C day^{-1} between 20 and 30 km. Above 30 km, no significant variation of cooling rates is found when a 3 km cirrus is present in the atmosphere. Further, for internal cooling we obtain a cooling rate of -8° C day^{-1}. For purposes of comparison, we also depict in Fig. 5b cooling rates derived from the band-by-band method employing a three-layer cloud model.

Strong cooling (~10°C day^{-1}) at the cloud top and rigorous warming (~6°C day^{-1}) near the cloud base are especially noticeable. The balance between the upward and downward fluxes near the cloud center results in a near zero cooling rate. The broadband cooling rate -8°C day^{-1} coupled with ~1°C day^{-1} warming at the cloud base appear to be consistent with the results derived from the band-by-band method.

Other atmospheric profiles also have been employed in performing broadband and band-by-band infrared cooling calculations. Similar agreements between the parameterized broadband and band-by-band methods were found. Finally, it should be pointed out that the present infrared parameterization scheme involving nonblack clouds simplifies the intricate cloud interactions with atmospheric infrared fluxes in terms of the broadband cloud radiative properties. The numerical effort and computational time requirement are consequently equivalent to those of clear-column cases.

Section 3

SOLAR RADIATION PROGRAM

3.1 Clear Atmosphere

In a clear atmosphere, we consider that Rayleigh scattering due to air molecules is insignificant above a height z_1 of 10 km for the downward solar flux. On the other hand, however, the upward solar flux above this height is contributed from the Rayleigh reflection upward plus a diffuse reflection component resulting from multiple reflections between the Rayleigh layer and the underlying surface. Hence, the downward and upward solar fluxes at level z above z_1 may be expressed by

$$F^{\downarrow}(z) = \mu_0 S_0 [1 - A(z_T - z)] , \tag{3.1}$$

$$F^{\uparrow}(z) = F^{\downarrow}(z_1) (r_a + G \bar{t}_a) [1 - \bar{A}(z - z_1)] , \tag{3.2}$$

where z_T is the height at the top of the atmosphere, the solar constant S_0 is taken to be 1353 W m^{-2}, and the cosine of the solar zenith angle is defined by

$$\mu_0 = \sin\theta \sin\delta + \cos\theta \cos\delta \cos\Delta , \tag{3.3}$$

where θ is the latitude, δ denotes the inclination angle, which is a function of the day of the year, and Δ is the hour angle. The flux reflection r_a and transmission t_a due to Rayleigh scattering is taken to be $r_a = 0.28 / (1 + 6.43 \mu_0)$ (Lacis and Hansen, 1974) and $t_a = 1 - r_a$ and $\bar{r}_a$ and $\bar{t}_a$ are the corresponding diffuse (or global) values which

are to be obtained from integrating μ_0 over the upper hemisphere. The gaseous broadband solar absorptivity A(z) will be defined later and its diffuse value $\bar{A}(z) = A\,[d\,u(z)]$ where d = 1.66 for H_2O and 1.9 for O_3. The higher diffusivity factor d for ozone is chosen to account for Rayleigh scattering effects on the ozone absorption. Based on a simple adding procedure the multiple reflections involving the Rayleigh scattering layer and the surface having a Labertian albedo of r_s are described by a non-dimensional upward diffuse component given by

$$G = t_a\, r_s\, (1 - \bar{r}_a\, r_s \cdot \bar{t}_a^2)^{-1} \,. \tag{3.4}$$

In Eq. (3.2), the r_a term represents the direct reflection of the downward solar flux while $G\,\bar{t}_a$ denotes the diffuse reflection component. Likewise, the downward and upward fluxes at heights below z_1 may be expressed by

$$F^{\downarrow}(z) = \mu_0\, S_0\, [1 - A(z_T - z)] \,, \tag{3.5}$$

$$F^{\uparrow}(z) = F^{\uparrow}(z_1)\, [1 + \bar{A}(z_1 - z)] \,, \tag{3.6}$$

It should be noted that Rayleigh scattering below z_1 will reduce both upward and downward fluxes by the same amount since its overlap with gaseous absorption in the near infrared may be neglected. Thus, the net flux and hence the heating rate may be evaluated without the incorporation of Rayleigh scattering.

Three absorbers are considered in the transfer of solar radiation, i.e., water vapor, carbon dioxide and ozone with the former two gases responsible for absorption in the near solar infrared region and the latter in the UV region. It is assumed that overlap of H_2O and CO_2

absorption and O_3 absorption is insignificant so that the broadband solar absorptivity may be expressed by

$$A(z) = \sum_i A_i(u_0/\mu_0)\, f_i + \sum_i A_i(u_w/\mu_0)\, f_i + \varepsilon\, A_5(u_c/\mu_0) \ , \qquad (3.7)$$

where u_o, u_w and u_c represent, respectively, path lengths for O_3, H_2O and CO_2, and f_i are the fractional solar flux associated with the individual band absorptivities A_i. The H_2O-CO_2 overlap correction is given by $\varepsilon = a + b\, A_5(u_w)$ where a and b are empirical constants derived from the measured data presented by Howard et al. (1956); a = 0.75 and b = -0.3/200 for $A_5(u_w) \geq 300$ cm^{-1}, and a = 1 and b = -0.7/300 for $A_5(u_w) < 300$ cm^{-1}. The individual absorptivity for ozone is given by

$$A_i(u_0/\mu_0) = 1 - \exp\,(-k_i\, u_o/\mu_0) \ , \qquad (3.8)$$

where k_i denote the ozone absorption coefficients taken from the data obtained by Inn and Tanaka (1953) and Vigroux (1953) and u_o is in units of cm NTP^{-1}. These coefficients and fractional solar fluxes are tabulated in Table 3. For water vapor and carbon dioxide, the empirical band equation derived by Liou and Sasamori (1975) is used. It has the following analytic form

$$A_i(u/\mu_0) = \frac{1}{\Delta\nu_i}\left[C_i + D_i \log_{10}\left(\frac{u}{\mu_0}\,\overline{P}^{\eta_i} + \chi_{0i}\right)\right] \ , \qquad (3.9)$$

where $\Delta\nu_i$ are the band widths, C_i, D_i, η_i and χ_{0i} are empirical constants. These constants are listed in Table 4. The pressure P in units of mm Hg is weighted over the path length given by $\overline{P} = \int_0^u P(u)\, du/u$ where u_w or u_c is in units of g cm^{-2}.

3.2 Cloudy Atmosphere

As in the case of the infrared radiation program, we consider a general two-layered cloud system. We wish to obtain the upward and downward solar fluxes at levels above the high cloud, between the high

Table 3. Ozone Absorption Coefficients and Fractional Solar Fluxes

$\Delta\lambda$ (μm)	i	k_i (-44° C)	f_i (Wm^{-2})*
0.20-0.21	1	9.8	1.24×10^{-4}
0.21-0.22	2	27	2.97×10^{-4}
0.22-0.23	3	75	4.59×10^{-4}
0.23-0.24	4	164	4.59×10^{-4}
0.24-0.25	5	254	5.14×10^{-4}
0.25-0.26	6	290	7.55×10^{-4}
0.26-0.27	7	241	1.35×10^{-3}
0.27-0.28	8	145	1.59×10^{-3}
0.28-0.30	9	33.7	6.46×10^{-3}
0.30-0.32	10	2.8	1.01×10^{-2}
0.32-0.34	11	0.16	1.50×10^{-2}
0.34-0.35	12	0.014	7.95×10^{-3}
0.45-0.50	13	0.0107	7.46×10^{-2}
0.50-0.55	14	0.055	6.78×10^{-2}
0.55-0.60	15	0.11	6.30×10^{-2}
0.60-0.65	16	0.09	5.87×10^{-2}
0.65-0.70	17	0.038	5.33×10^{-2}
0.70-0.80	18	0.015	9.14×10^{-2}

* Based on a solar constant of 1353 W m^{-2} and the fractional fluxes presented by Thekaekara (1974, 1976).

Table 4. Empirical Constants for H_2O and CO_2 Bands and Fractional Solar Fluxes.

$\lambda(\mu m)$	i	C_i	D_i	K_i	$\Delta\nu_i$ (cm^{-1})	f_i (Wm^{-2})*
H_2O band						
0.94	1	-135	230	125	1400	0.0760
1.1	2	-292	345	180	1000	0.0528
1.38	3	202	460	198	1500	0.0732
1.87	4	127	232	144	1100	0.0386
2.7	5	337	246	150	1000	0.0242
3.2	6	-144	295	151	540	0.0088
CO_2 band						
2.7	5	-137	77	68	320	0.0073

* Based on a solar constant of 1353 Wm^{-2} and the fractional fluxes presented by Thekaekara (1974, 1976).

and low clouds and below the low cloud. Utilizing the approach similar to the flux transfer in a clear atmosphere and in reference to Fig. 1, the downward and upward solar fluxes above z_{t1} may be written in the form

$$F^{\downarrow}(z) = \mu_0 \, S \, [1 - A(z)] \, , \tag{3.10}$$

$$F^{\uparrow}(z) = F^{\downarrow}(z_{t1}) \, R_3 \, [1 - \bar{A}(z - z_{t1})] \, , \qquad z > z_{t1} \tag{3.11}$$

where R_3 is the solar flux reflection involving the two cloud system and the surface defined below and $F^{\downarrow}(z_{t1})$ is the downward solar flux at position z_{t1}.

To derive the flux from below the high cloud, we let the solar flux reflection and transmission for the high (1) and low (2) clouds be (r_1,t_1) and (r_2,t_2), respectively, with their corresponding diffuse (or global) quantities denoted as $\bar{r}_1$, $\bar{t}_1$, $\bar{r}_2$ and $\bar{t}_2$ where

$$\begin{matrix} \bar{r} \\ \bar{t} \end{matrix} \left\{ \right. = 2 \int_0^1 \begin{matrix} r(\mu_0) \\ t(\mu_0) \end{matrix} \left. \right\} \mu_0 \, d\mu_0 \, . \tag{3.12}$$

Moreover, we also let A_1 and A_2 be the diffuse gaseous absorption between the high and low clouds and between the low cloud and the surface. We also utilize a non-dimensional total upward generation function $G_2^{(t)}$ which is initiated from the reflection of the low cloud with a contribution from the surface to be defined below. Thus, the downward and upward fluxes between z_{b1} and z_{t2} may be written

$$F^{\downarrow}(z) = F^{\downarrow}(z_{t1}) \, [t_1 + G_2^{(t)} \, (1 - \bar{A}_1) \, \bar{r}_1] \, [1 - \bar{A}(z_{b1} - z)] \, , \tag{3.13}$$

$$F^{\uparrow}(z) = F^{\downarrow}(z_{t1})\, G_2^{(t)}\, [1 - \bar{A}(z - z_{t2})]\,, \qquad (3.14)$$
$$z_{b1} > z > z_{t2}$$

In Eq. (3.13), the t_1 term represents the direct transmission of the broadband solar flux reaching the high cloud top, while the following term denotes the diffuse component which is generated through the generation function $G_2^{(t)}$.

Similarly, if we let the direct transmission for the two cloud system be T_2 (the corresponding reflection will be denoted by R_2) and the upward generation function originating from the surface be G_3, then the downward and upward fluxes below the low cloud base z_{b2} are described by

$$F^{\downarrow}(z) = F^{\downarrow}(z_t)\, T_3\, [1 - \bar{A}(z_{b2} - z)]\,, \qquad (3.15)$$

$$F^{\uparrow}(z) = F^{\downarrow}(z_t)\, G_3\, [1 - \bar{A}(z)]\,, \qquad (3.16)$$
$$z_{b2} > z > 0$$

where T_3 denotes the direct transmission for the system of two clouds and the surface.

The derivation of the flux reflection and transmission and the upward generation function for multiple cloud layers is similar to the adding method for radiative transfer (see, e.g., Liou, 1980; Hansen, 1971) except that we have separated the direct (associated with μ_0) and diffuse components for the transmitted beam. In this approach we postulate that the broadband solar flux either in the form of direct or diffuse beam is additive by means of multiple reflections between layers concerned. Thus, the flux reflection and transmission for two

cloud layers are

$$R_2 = r_1 + G_2 (1 - \bar{A}_1) \bar{t}_1 , \tag{3.17}$$

$$T_2 = t_1 (1 - \bar{A}_1) t_2 + G_2 (1 - \bar{A}_1)^2 \bar{r}_1 \bar{t}_2 , \tag{3.18}$$

where the first and second terms represent, respectively, the direct and diffuse contribution with the latter resulted from the upward generation function from the low cloud layer given by

$$G_2 = t_1 (1 - \bar{A}_1) r_2 [1 - (1 - \bar{A}_1)^2 \bar{r}_1 \bar{r}_2]^{-1} , \tag{3.19}$$

with the last term denoting multiple reflections between two clouds. It follows that the reflection and transmission for a combination of two clouds and the surface is then given by

$$R_3 = R_2 + G_3 (1 - \bar{A}_2) \bar{T}_2^* , \tag{3.20}$$

$$T_3 = T_2 + G_3 (1 - \bar{A}_2) \bar{R}_2^* , \tag{3.21}$$

where the upward generation function from the surface is

$$G_3 = T_2 (1 - \bar{A}_2) r_s [1 - (1 - \bar{A}_2)^2 \bar{R}_2^* r_s]^{-1} , \tag{3.22}$$

and $\bar{R}_2^*$ and $\bar{T}_2^*$ are the diffuse reflection and transmission for the two cloud system when radiation is incident from below. Thus, Eqs. (3.17) - (3.19) may be modified to yield

$$\bar{R}_2^* = \bar{r}_2 + G_2^* (1 - \bar{A}_1) \bar{t}_2 , \tag{3.23}$$

$$\bar{T}_2^* = \bar{t}_2 (1 - \bar{A}_1) \bar{t}_1 + G_2^* (1 - \bar{A}_1)^2 r_2 \bar{t}_1 , \tag{3.24}$$

$$G_2^* = \bar{t}_2 \, (1 - \bar{A}_1) \, \bar{r}_1 \, [(1 - \bar{A}_1)^2 \, \bar{r}_1 \, \bar{r}_2]^{-1} \, . \qquad (3.25)$$

Finally, in Eqs. (3.13) and (3.14), the total upward generation function contributed from the low cloud and the surface is

$$G_2^{(t)} = G_2 + G_3 \, (1 - \bar{A}_2) \, \bar{t}_2 \, [1 - \bar{A}_1)^2 \, \bar{r}_1 \, \bar{r}_2]^{-1} \, , \qquad (3.26)$$

where the second term is required in order to give proper internal fluxes.

In the case of one cloud layer, only Eqs. (3.10) - (3.14), (3.17) and (3.19) are applicable. In this case, the total diffuse generation function $G_2^{(t)}$ in Eqs. (3.13) and (3.14) should be replaced by the value G_2 defined in Eq. (3.19) and the total reflection at the top of the cloud system R_3 should be replaced by the value R_2 defined in Eq. (3.17).

The broadband solar reflection and transmission values for various cloud types are obtained through the following parameterization equation based on detailed radiative transfer calculations:

$$r,t(\mu_0,W) = \sum_{m=0}^{3} \sum_{n=0}^{3} b_{mn} \, \mu_0^m \, W^n \qquad (3.27)$$

where b_{mn} are empirical coefficients derived based on the parameterization principle proposed by Liou and Wittman (1979), and the vertical liquid content W is in units of 10^2 g m^{-2}. The b_{mn} for Cu, As, St and Ci are respectively given in Tables 3, 4, 5 and 6 of that paper. Finally, computations of solar heating rates in clear, overcast and partly cloudy conditions follow Eqs. (2.20) and (2.21).

3.3 Verification of Solar Parameterization Program

In this section, we present some results calculated from the solar

parameterization program described in previous sections. Comparisons will also be made with results computed from a more exact and comprehensive radiative transfer program developed at the University of Utah over the last few years (Freeman and Liou, 1979; Liou and Wittman, 1979).

In Fig. 6 (Liou and Ou, 1983) are shown the comparisons of the solar net fluxes and heating rates computed from the parameterization scheme and a more exact and comprehensive transfer program. A fraction of daytime of 0.5 along with values depicted in the diagram are used in the computation. Agreement between these two methods is within ~0.02°C day^{-1} (solar day is used here) and 5 W m^{-2} for solar heating rates and net fluxes, respectively. Below about 10 km, solar heating is basically produced by absorption of H_2O. Between about 10-15 km, absorption of CO_2 contributes to within about 0.1°C day^{-1} heating rates. Above 15 km, large solar heating is exclusively caused by O_3 absorption. The net solar flux ranges from about 350 W m^{-2} at the top of the atmosphere to about 270 W m^{-2} at the surface. A series of comparisons between the parameterization and more exact programs involving different atmospheric conditions and solar zenith angles have also been performed. We found that the present parameterization program for net flux and heating rate computations, which has not been presented in our previous publications, has an accuracy similar to the case depicted here.

Next, we compare the net solar flux and heating rate profiles in cloudy atmospheres computed from the present parameterization program with those obtained from a more exact radiative transfer calculation. In Fig. 7 (Hutchison and Liou, 1983) a 1 km single cumulus cloud was inserted into a midlatitude winter atmosphere with a base height of

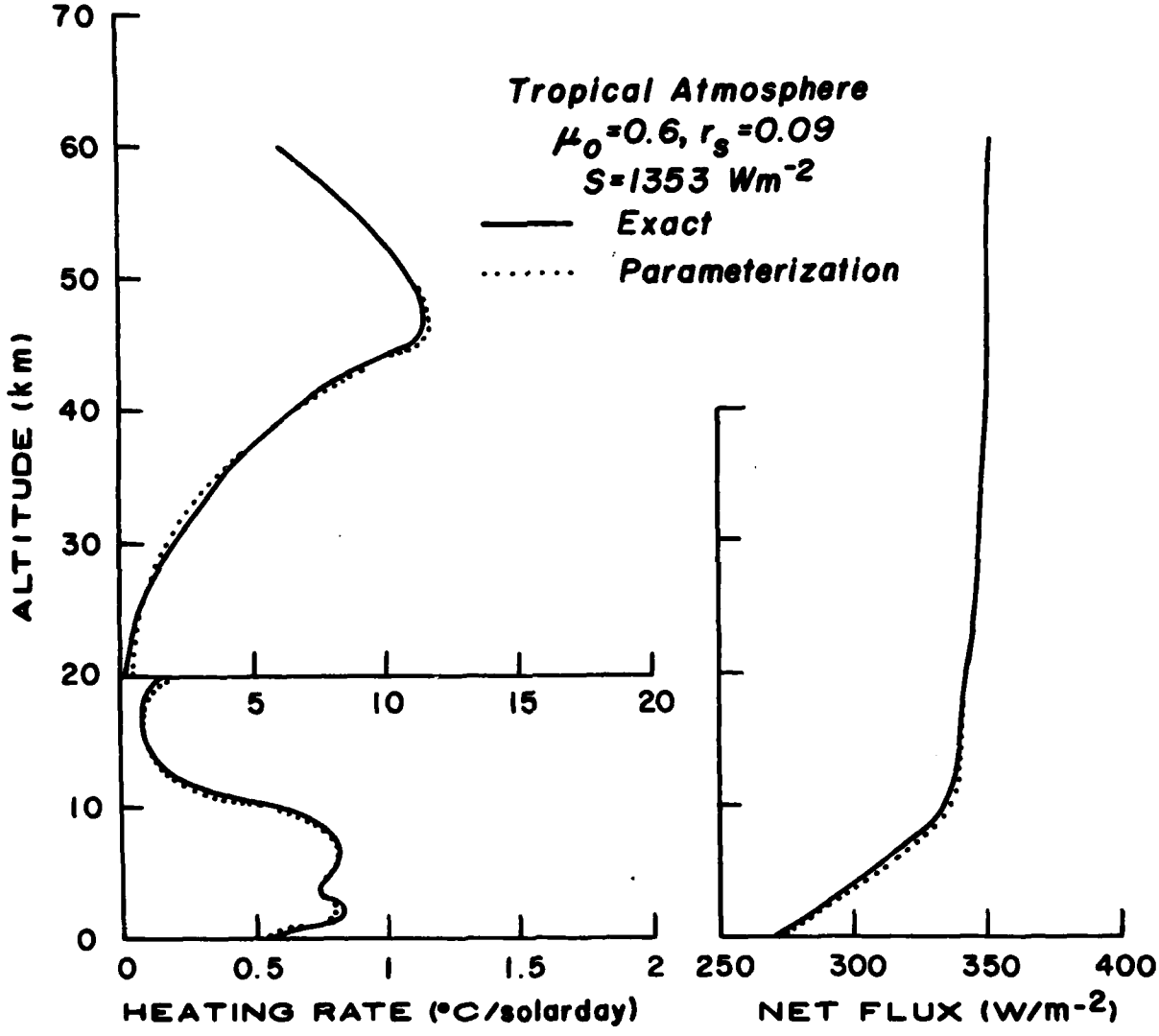

Fig. 6 Comparisons of solar heating rates and net fluxes computed from the flux parameterization scheme with results from a more exact radiative transfer program.

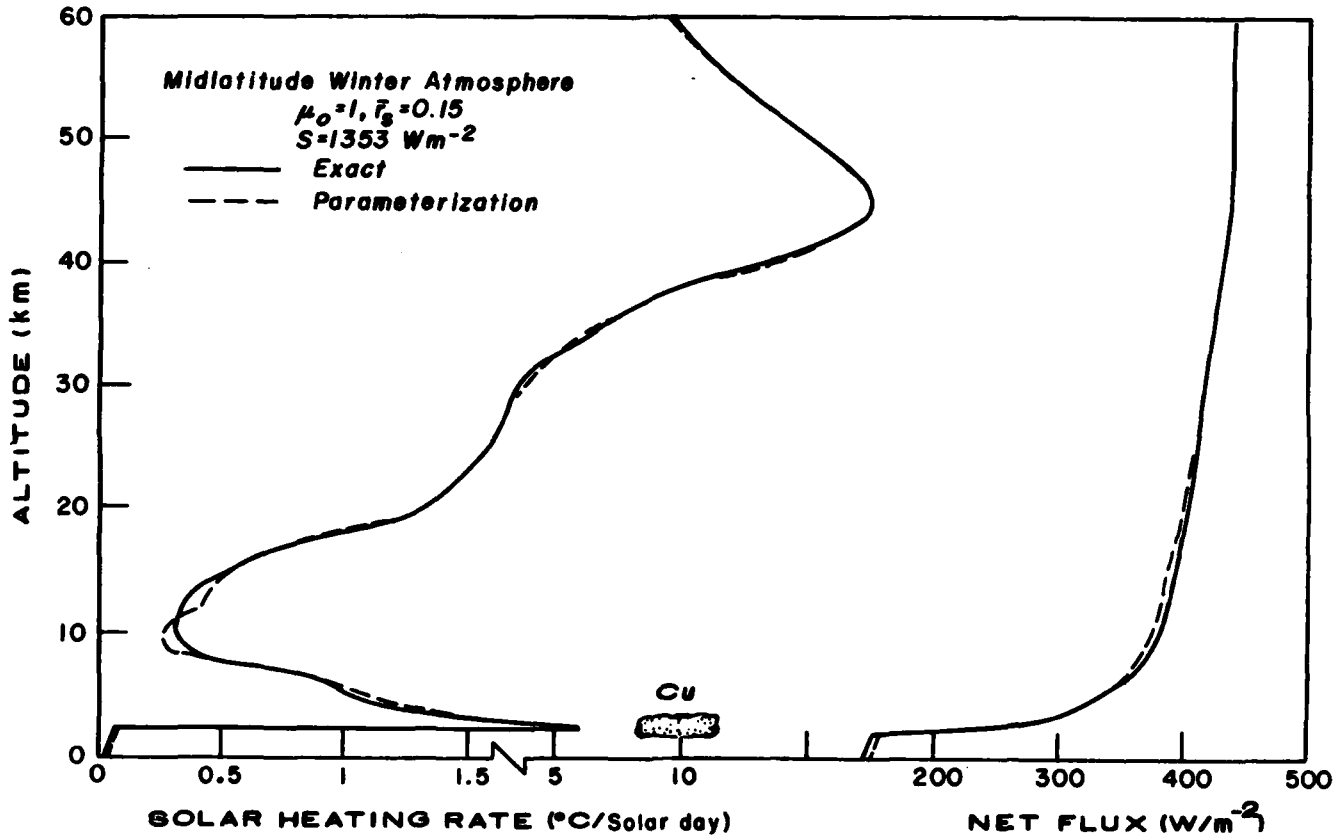

Fig. 7. Heating rate and net flux profiles in a midlatitude winter atmosphere containing a single cumulus (2-3 km) cloud.

2 km. A cosine of the solar zenith angle of 1, a surface albedo of 0.15 and a solar constant of 1353 W m^{-2} were used in the calculation. The fractional duration of sunlight used was 0.5 in this exercise. Agreements of heating rate and net flux profiles between the parameterization method and a more exact method are generally excellent in the cumulus case. The presence of a low cloud clearly alters the solar heating profile above and below the cloud. A heating rate of more than 10°C/24 hr is produced by a 1 km cumulus cloud, whereas heating rates are greatly suppressed between the cloud and the surface. Similar results and comparisons are shown for the middle cloud case depicted in Fig. 8. Because of the larger liquid water content in the altostratus than that in the cumulus, a larger heating rate is produced, coupled with a greater reduction of the net solar flux available at the surface.

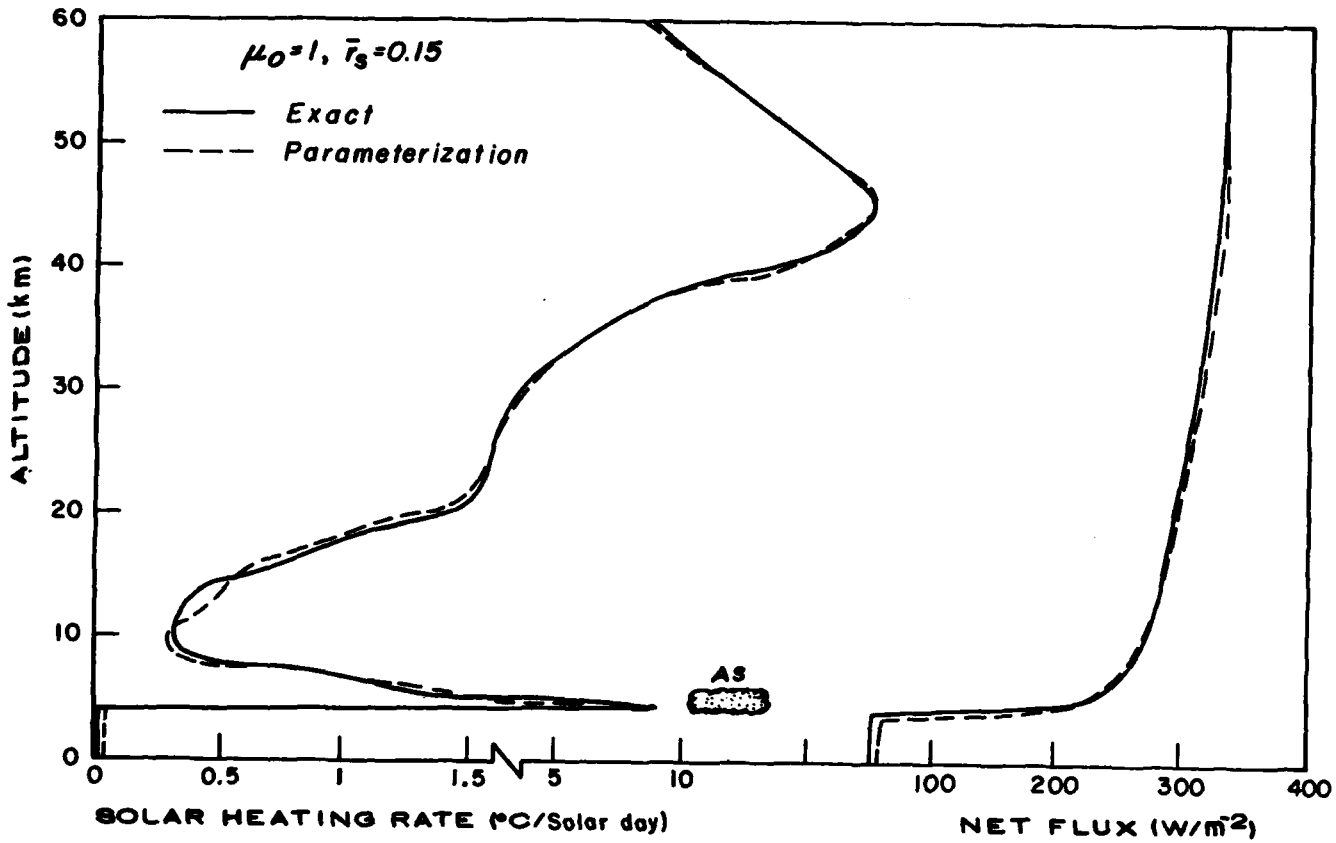

Fig. 8. Heating rate and net flux profiles in a midlatitude winter atmosphere containing a single altostratus (4-5 km) cloud.

Section 4

PRELIMINARY GLOBAL RADIATION AND CLOUD RESULTS

4.1 Global Cloud Cover

In order to test the applicability of radiation programs to all atmospheric conditions, a cloud formation scheme was used in connection with the AFGL six-layer general circulation model. The scheme is similar to that proposed by Liou and Zheng (1984). From the model relative humidity defined as $h = q/q_s(T)$, where q and T are specific humidity and temperature, respectively, criteria for cloud formation and fractional cloud cover are devised on the basis of empirical-statistical means. When the predicted relative humidity h is greater than a prescribed value, it is assumed that the water and/or ice cloud may be formed with the cloud cover computed from an empirical equation, whereas if h is smaller than or equal to the prescribed value, no cloud is allowed to form. Thus,

$$C = \begin{cases} g(h) , & h > h_c \\ 0 , & h \leq h_c \end{cases} \tag{4.1}$$

where

$$g(h) = \{[h - h_c(\sigma)] / [1 - h_c(\sigma)]\}^2 \tag{4.2}$$

and the critical relative humidity as a function of σ is given by

$$h_c(\sigma) = \sum_{n=0}^{3} a_n \sigma^n \tag{4.3}$$

where $\sigma = P/P_*$, P_* the surface pressure, and the a_n are empirical coefficients having values of $a_0 = 1$, $a_1 = -0.218$, $a_2 = -0.3196$, and $a_3 = 3.464$. In reference to Fig. 9 and subject to the above conditions, clouds are permitted to form on layers σ_5, σ_4 and σ_3. In cases of multi-layered clouds, the total cloud cover is calculated by means of a minimum overlap scheme, i.e., the largest cloud cover obtained will be the total cloud cover.

Utilizing the initial field of 0000 Z, 15 January 1978, consisting of temperature and specific humidity provided to us by AFGL, cloud fields are generated. It should be noted that no prediction is performed in this exercise. On this day, IR cloud pictures for the northern hemisphere from the NOAA satellite were available. Depicted in Fig. 10a is an IR cloud picture covering the time period from 0756 Z, 14 January 1978 to 0756 Z, 15 January 1978 for vertification of the model cloud generation. Three frontal band clouds are seen in the Pacific ocean. In addition, large cloud covers are also observed on the eastern part of the United States and Canada and over the Asian continent. Clouds associated with the intertropical convergence zone are visible in the tropical regions. The computed cloud covers illustrated in Fig. 10b generally agree well with the cloud patterns seen from the satellite, except in the tropical regions located at about 120° W and 60° E where overestimates of the cloud cover are seen. In this presentation, the minimum cloud cover contour line is 20% and shaded areas represent cloud covers greater than 50%. This good comparison between the computed and satellite observed IR cloud covers is quite encouraging.

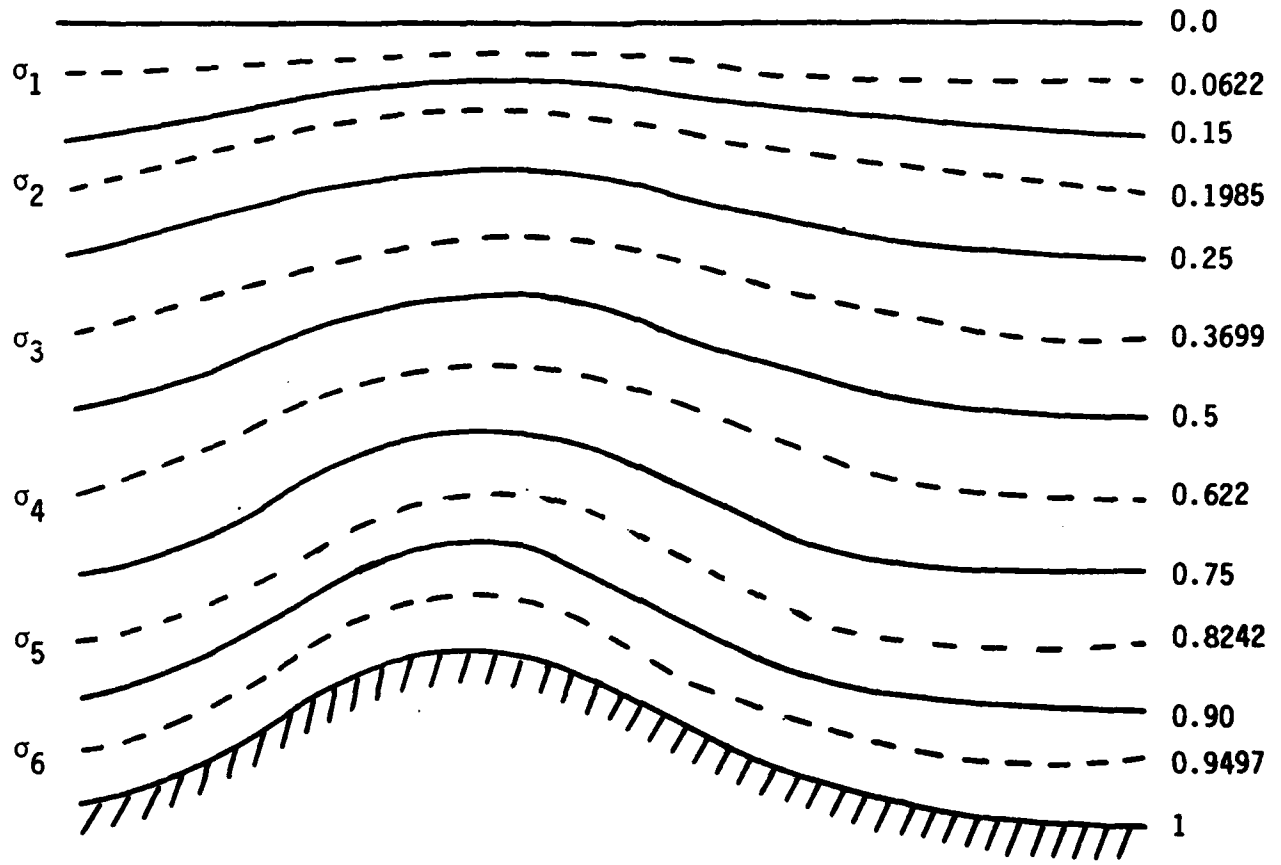

Fig. 9 AFGL six-layer model. Clouds are permitted to form on layers σ_5, σ_4 and σ_3.

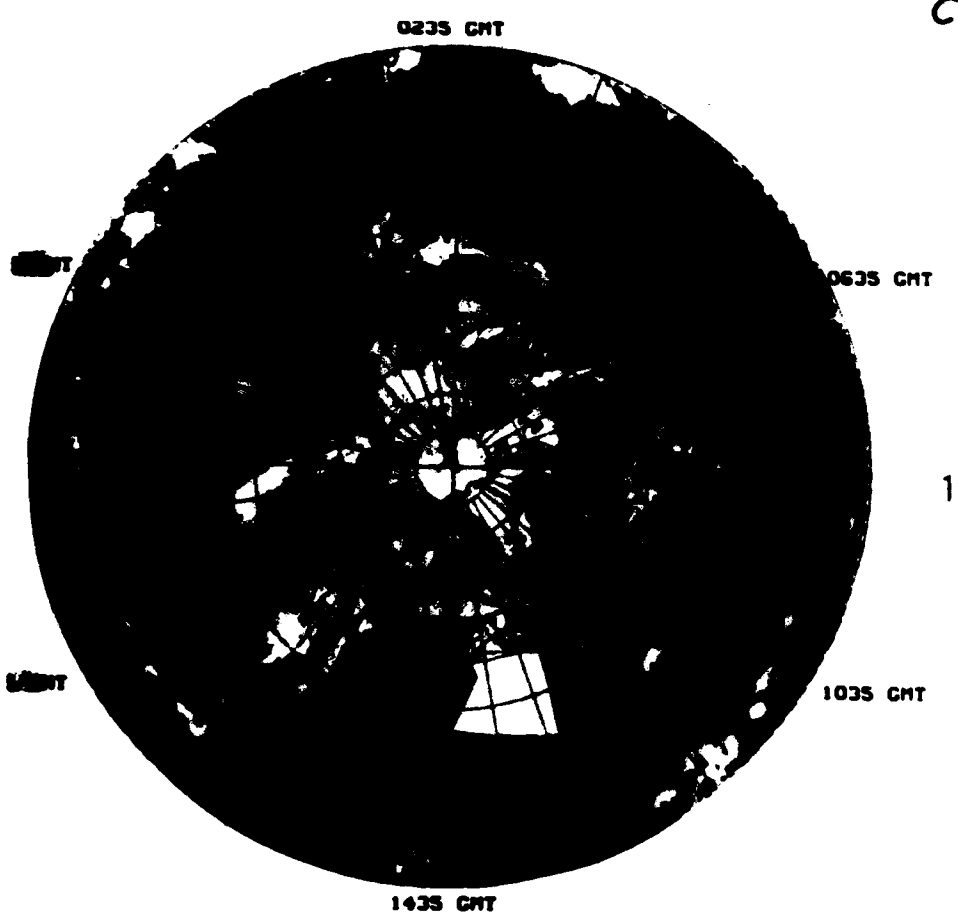

Fig. 10a. The IR cloud picture from the NOAA satellite on 15 January 1978.

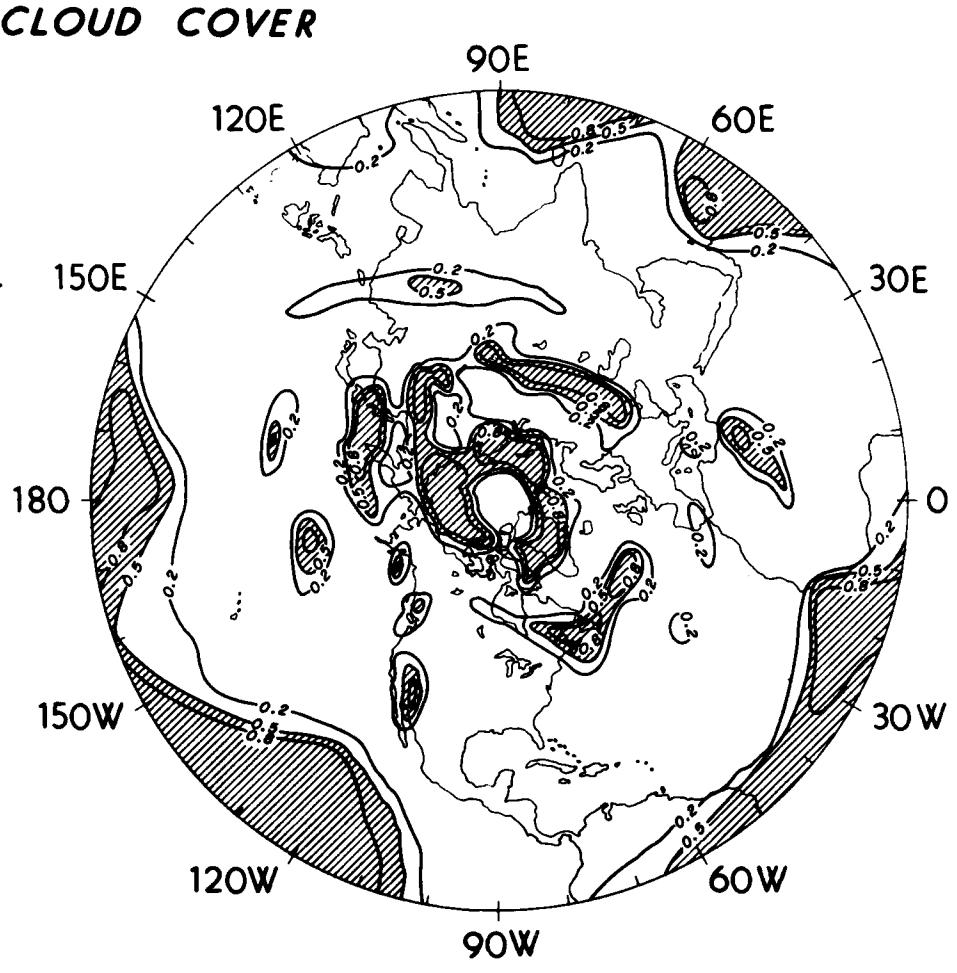

Fig. 10b. The cloud cover (shaded areas) computed from the AFGL six-layer baseline spectral model with the UU cloud formation scheme.

4.2 Global Radiation Budget

Using the AFGLGCM with the incorporation of UU radiation programs and the aforementioned initial data, global distributions of outgoing IR and reflected solar fluxes at the model top were generated and they are illustrated in Figs. 11 and 12. The IR and solar flux contours are in units of W m^{-2}. In Fig. 12, regions above the zero line denote the solar night. For comparison purposes, global cloud cover distributions are also presented (Fig. 13). Generally, lower IR fluxes are associated with colder cloud fields. On the other hand, cloud fields also produce larger reflected solar fluxes. Since these results are preliminary and since the prime objective of these illustrations is to demonstrate that the present radiation/cloud programs in the context of AFGLGCM are functioning, detailed physical interpretations of these graphs will not be given here.

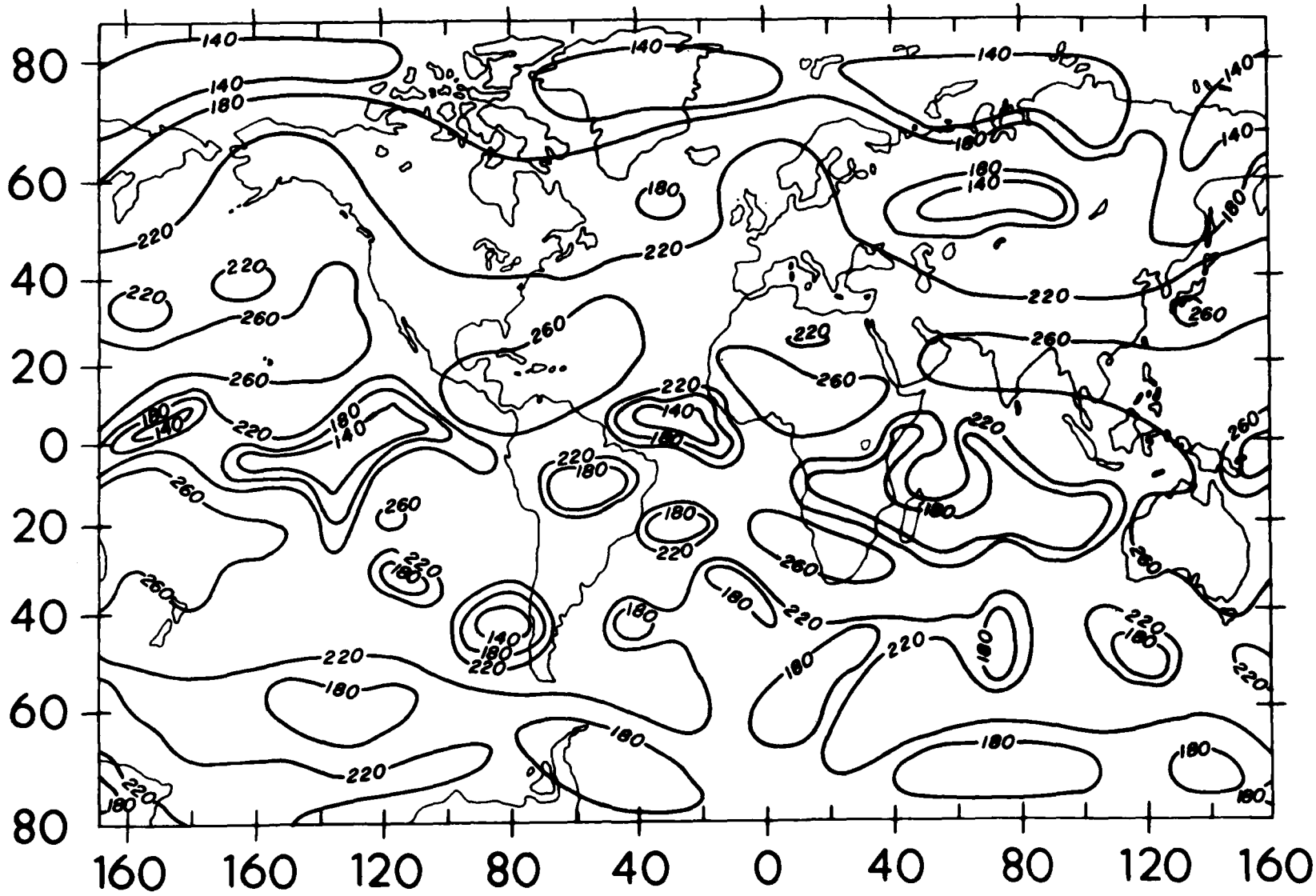

Fig. 11. The computed global distributions of outgoing IR fluxes (in units of W m^{-2}) at the top of the AFGL six-layer spectral model on 15 January 1978.

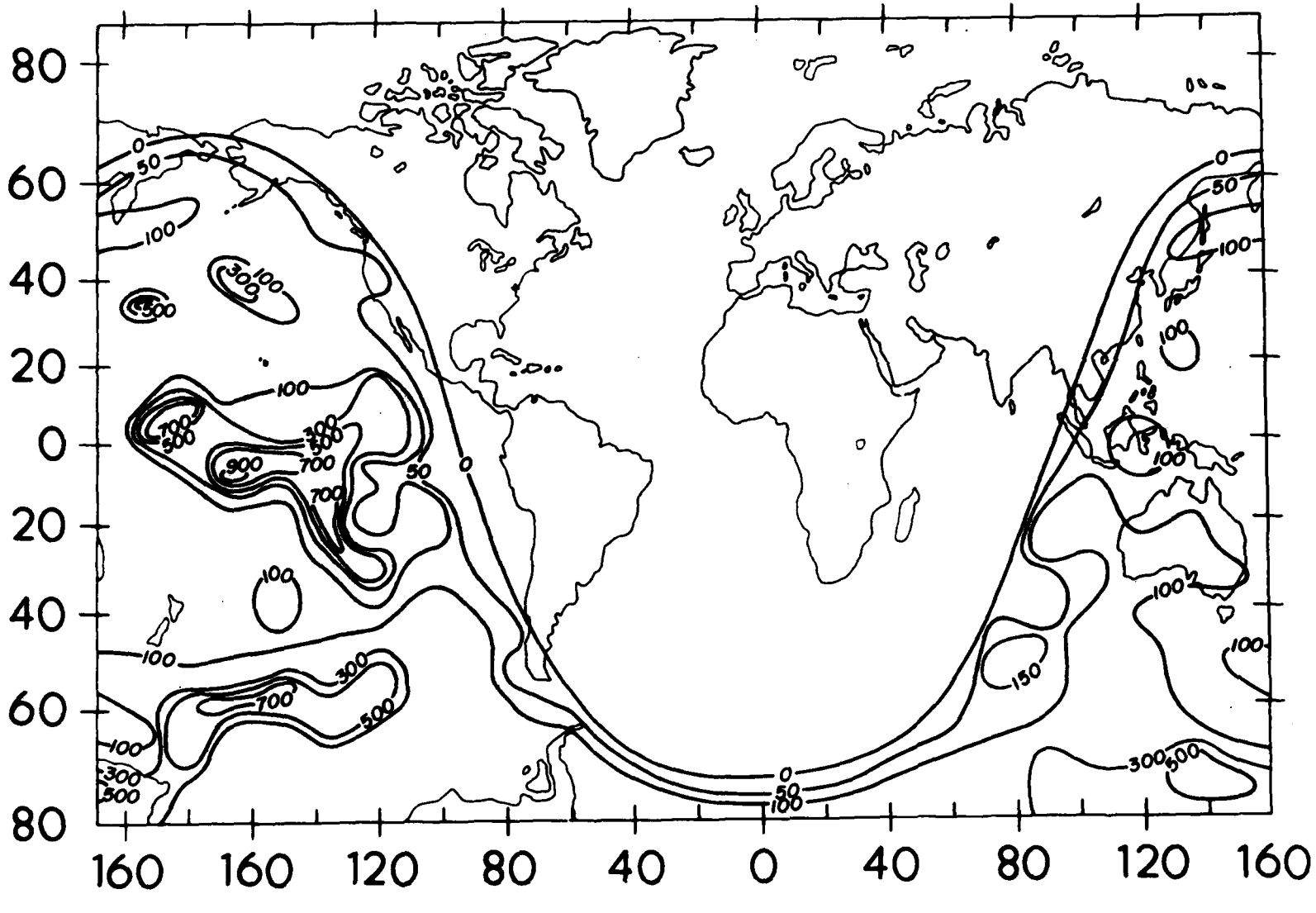

Fig. 12. Computed global distributions of reflected solar flux (in units of W m^{-2}) at the top of the AFGL six-layer spectral model on 15 January 1978.

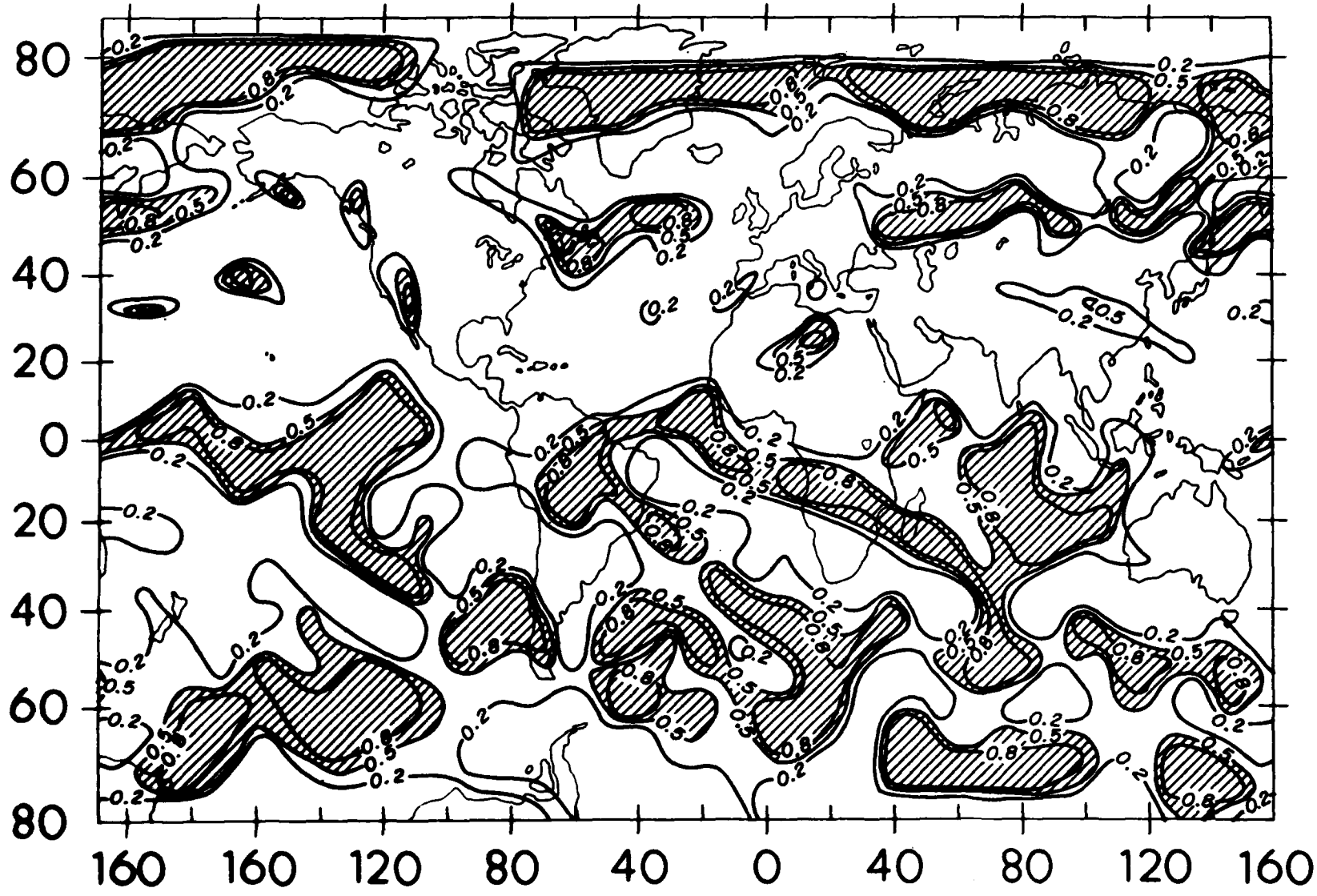

Fig. 13. Computed global cloud covers (shaded areas) on 15 January 1978.

Section 5

SUMMARY

In this report we have summarized the infrared and solar radiation parameterization programs developed at the University of Utah. The infrared radiation parameterization utilizes the broadband emissivity approach in which the emissivity for the individual absorption band is derived either from band models (water vapor and ozone) or line-by-line data (carbon dioxide). We have also presented basic flux equations for an atmosphere containing high and low clouds. High clouds are treated as non-black whose broadband emissivity, transmissivity and reflectivity are parameterized in terms of the vertical ice content. On the solar side, parameterization has been carried out by developing a broadband absorptivity for water vapor, carbon dioxide and ozone absorption. In line with this, cloud reflection and transmission properties are parameterized in terms of the liquid water content and solar zenith angle. Based on broadband solar radiative properties for gases and clouds, we have devised equations for the computation of upward and downward fluxes for clear and one- and two-layered cloudy atmospheres. We have presented in some detail basic parameterized equations and relevant coefficients and/or constants used in the current version of the radiation code. Accuracies of all the parameterization programs have been verified via more comprehensive and exact radiative transfer calculations described in this report.

Moreover, we have provided a comprehensive documentation of the radiation parameterization programs and listings of all the relevant computer formats for use in general circulation models. Specifically, we have described in some detail the link and interface between the UU radiation-cloud programs and the AFGL six-layer spectral model. We have also presented some preliminary results of the global distributions of clouds and outgoing IR and reflected solar fluxes generated from the AFGL six-layer spectral model with the incorporation of UU radiation-cloud parameterization programs.

Appendix

DOCUMENTATION OF RADIATION PARAMETERIZATION PROGRAMS

A.1 General Description of the Programs

The basic principles of calculating both IR and solar radiation fluxes and heating rates have been illustrated in Sections 2 and 3. In this section, we document the detailed computer routines for the IR and solar parameterization programs for use in general circulation models.

The entire radiation program is composed of four subroutines denoted as PRERAD, IRRAD, IRCLR and IRCLD. The subroutine PRERAD serves as a driver program which connects the main part of radiation calculations with other GCM programs. It interpolates the model-generated temperature and humidity profiles from the main part of the GCM on the layers designed for radiation calculations. The program also determines the cloud position along with the cloud fraction and thickness. The computed radiative heating rates for radiation layers from the subroutine IRRAD are then weighted by density to get the mean radiative heating rate for each GCM layer.

The subroutine IRRAD is the main program for radiation calculations. It is composed of IR and solar parts. In the IR part, the path lengths in pressure coordinates are first computed and then adjusted in accordance with a number of temperature and pressure correction schemes denoted in Section 2. Next, the coefficients of the third-order

polynomial for IR emissivities are obtained by interpolation between the prescribed reference temperatures listed in Table 1. The IR program is then connected to a large computational loop in which the radiative fluxes for each cloud configuration are calculated based on the following three atmospheric conditions:

a. For a clear sky, the subroutine IRCLR is called.

b. For low or middle clouds, the subroutine IRCLR is called twice for regions above and below the cloud.

c. For a high (cirrus) cloud, the subroutine IRCLD is called once.

Lastly, in the IR program, the total heating rate profile is obtained from the net flux divergence using a centered finite difference scheme.

In the solar part, the path lengths of each model layer for water vapor, carbon dioxide and ozone are first computed. These layered path lengths are then substituted into equations for the computations of gaseous absorptivities. Again, the solar program is also connected to a large computational loop in which the solar net fluxes for each cloud configuration are computed according to the following atmospheric conditions:

a. For a clear sky, the solar fluxes are obtained using the previously computed absorptivities with Rayleigh scattering corrections given in Section 3.

b. For cloudy conditions, cloud reflectivity, transmissivity and absorptivity are first computed utilizing formulas proposed by Liou and Wittman (1979). The net solar flux for each radiation layer is computed according to formulas given in Section 3.

In the final portion of the solar part, the solar heating rate is computed from the net flux divergence using a centered finite difference scheme.

The subroutine IRCLR computes the IR fluxes in clear regions. Thus, it can be used to compute the entire clear column between model top and surface, the clear region between the low or middle cloud bottom and surface, or the region above the cloud. The subroutine IRCLD computes the IR fluxes in a column containing only one layer of a non-black cloud. It is applicable to a single non-black cloud confined either between the surface and model top or between the black cloud top and model top. The computational procedure is similar to that described in IRCLR. However, the flux components required in IRCLD are four in both the above-cloud and below-cloud regions. These four components include two emitted fluxes in upward and downward directions, one reflected flux, and one transmitted flux. The advantage of the method used here is that all these components can be computed based on one generalized formula. Consequently, the programming burden is greatly reduced, and the program if further vectorized can become extremely efficient.

A.2 Interfacing with AFGLGCM

A schematic flow diagram illustrating the connection between the AFGLGCM (Brenner et al., 1982) and radiation programs is depicted in Fig. 14. Two separate subroutines referred to as ZENITH and CLOUD are also connected to AFGLGCM. The subroutine ZENITH computes the global distribution of the solar zenith angle while CLOUD computes the cloud cover distribution in the three cloud-forming model layers. Bascially, the major modifications

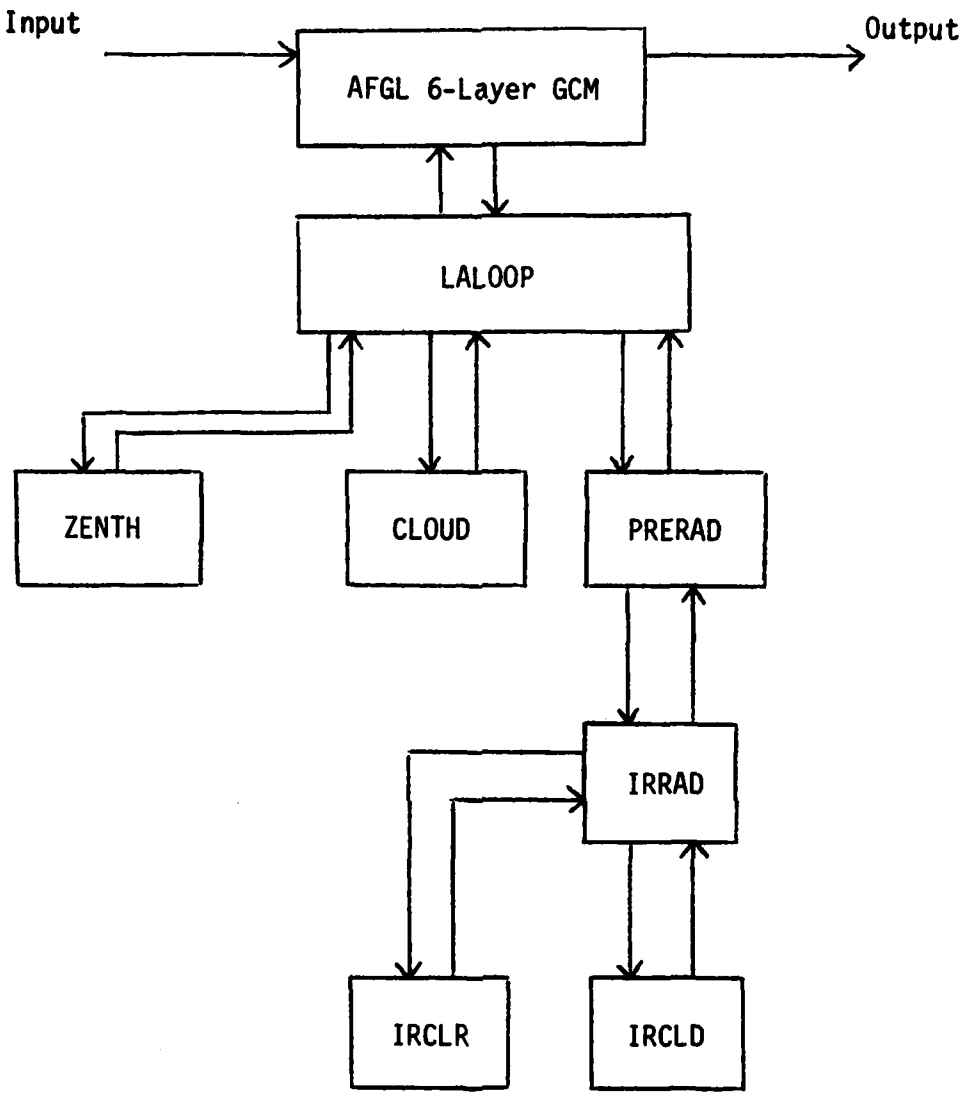

Fig. 14. A schematic flow diagram illustrating the interface of the AFGL 6-Layer GCM with the present radiation programs.

are all done in the subroutine LALOOP contained in AFGLGCM. Other minor modifications include (a) storing the surface albedo data in array SALB by a read statement in the main program, (b) adding statements in subroutine SPTOGP to compute surface pressures, and (c) inserting print statements to list the values of total heating rate, radiative heating rate, temperature humidity and surface pressure at selected grid points and time steps.

In the common block CZALB, SZ stores values of the cosine of the solar zenith angle and SALB stores surface albedo values. In the common block STORE, RADTEM stores global radiative heating rate data, ICL stores global cloud cover information, and KFLUX stores data for outgoing IR and reflected solar fluxes as well as net radiative fluxes at the top of the atmosphere. In the common block RADPGR, RIRAD stores data for radiative heating rates for two latitudinal circles described in LALOOP. Finally, in the common block ZONAV, YYY stores zonally averaged total and radiative heating rates, IYYY stores zonally averaged temperature and humidity values, and IPPP stores zonally averaged surface pressure values.

The basic executing procedures for the new radiation-AFGLGCM program are similar to those for the original AFGLGCM program. Also note that the new program has been tested and verified using the CRAY-1 computer in NCAR. Finally, the complete listings of the radiation subroutines PRERAD, IRRAD, IRCLR and IRCLD along with modified subroutines LALOOP, NLPROD, and SPTOGP in the AFGLGCM main program may be obtained from K.N. Liou at the University of Utah.

REFERENCES

Brenner, S., C.H. Yang and S.Y.K. Yee, 1982: The AFGL spectral model of the moist global atmosphere: Documentation of the baseline version. AFGL-TR-82-0393, Air Force Geophysics Laboratory, ADA129283.

Cox, S.K., 1969: Observational evidence of anomalous infrared cooling in a clear tropical atmosphere. J. Atmos. Sci., 26, 1347-1349.

Dickinson, R.E., 1973: Method of parameterization for infrared cooling between altitudes of 30 and 70 kilometers. J. Geophys. Res., 78, 4451-4457.

Ellingson, R.G. and J.C. Gille, 1978: An infrared radiative transfer model. Part I. Model description and comparison of observations with calculations. J. Atmos. Sci., 35, 523-545.

Fels, S.B. and M.D. Schwarzkopf, 1981: An efficient, accurate algorithm for calculating CO_2 15 μm band cooling rates. J. Geophys. Res., 86, No. C2, 1205-1232.

Goldman, A. and T.G. Kyle, 1968: A comparison between statistical model and line-by-line calculation with application to the 9.6 μm and 2.7 μm water vapor bands. Appl. Opt., 7, 1167-1177.

Hansen, J.E., 1971: Multiple scattering of polarized light in planetary atmospheres. Part I. The doubling method. J. Atmos. Sci., 28, 120-125.

Hutchison, K. and K.N. Liou, 1982: Parameterization of broadband solar radiation transfer in clear and cloudy atmospheres. Scientific Report, Air Force Geophysics Laboratory, AFGL-TR-82-0364, ADA123396.

Inn, E.C. and Y. Tanaka, 1953: Absorption coefficient of ozone in the ultraviolet and visible regions. J. Opt. Soc. Amer., 43, 870-873.

Lacis, A.A. and J.E. Hansen, 1974: A parameterization for the absorption of solar radiation in the earth's atmosphere. J. Atmos. Sci., 31, 118-133.

Liou, K.N., 1980: An Introduction to Atmospheric Radiation. Academic Press, 392 pp.

_____, and S.C. Ou, 1981: Parameterization of infrared radiative transfer in cloudy atmospheres. J. Atmos. Sci., 38, 2707-2716.

_____, and S.C. Ou, 1983: Theory of equilibrium temperature in radiative-turbulent atmospheres. J. Atmos. Sci., 40, 214-229.

_____, and T. Sasamori, 1975: On the transfer of solar radiation in aerosol atmospheres. J. Atmos. Sci., 32, 2166-2177.

_____, and G.D. Wittman, 1979: Parameterization of the radiative properties of clouds. J. Atmos. Sci., 36, 1261-1273.

_____, and Q. Zheng, 1984: A numerical experiment on the interactions of radiation, clouds and dynamic processes in a general circulation model. J. Atmos. Sci., 41, 1513-1535.

Manabe, S. and R. Strickler, 1964: Thermal equilibrium of the atmosphere with a given distribution of relative humidity. J. Atmos. Sci., 21, 361-385.

Ou, S.C. and K.N. Liou, 1983: Parameterization of carbon dioxide 15 μm absorption and emission. J. Geophys. Res., 88, 5203-5207.

Roberts, R.E., J.A. Selby and L.M. Biblerman, 1976: Infrared continuum absorption by atmospheric water vapor in the 8-12 μm window. Appl. Opt., 15, 2085-2090.

Rodgers, C.D. and C.D. Walshaw, 1966: The computation of infrared cooling in planetary atmospheres. Quart J. Roy. Meteor. Soc., 92, 67-92.

Vigroux, E., 1953: Contributions a l'étude experimentale de absorption d l'ozone. Ann. Phys., 8, 709-762.

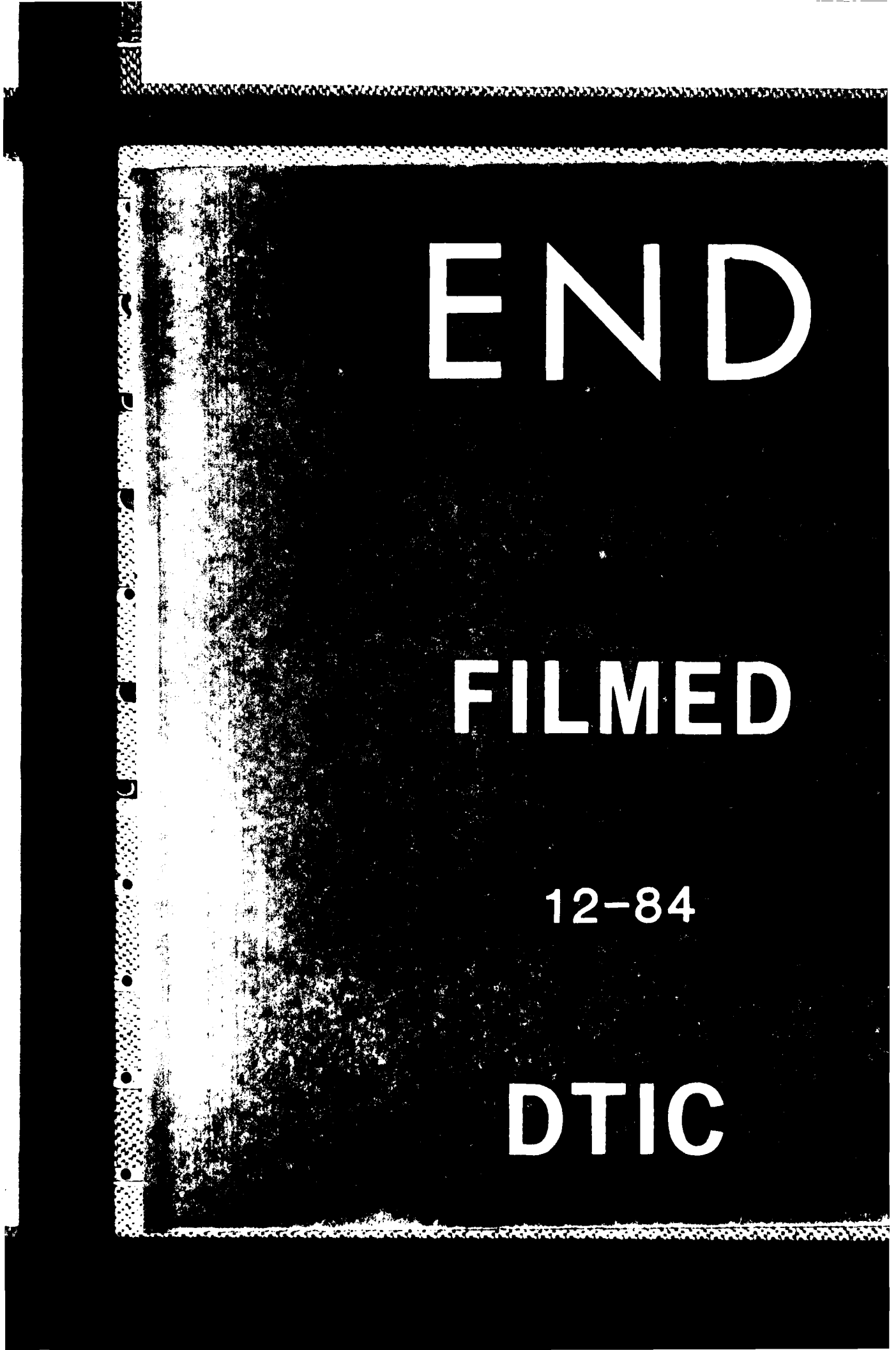
END
FILMED
12-84
DTIC